What's new?
One approach to immunotherapy is to engineer a patient/s own cytotoxic lymphocytes (CTLs) to express receptors for tumor-associated antigens. However, tumors often develop strategies to evade the anti-tumor activity of these immune cells. In this study using a mouse model of melanoma, the authors found that the efficacy of transgenic CTLs was blocked due to a massive accumulation of myeloid-derived suppressor cells (MDSCs) in the tumor. Surprisingly, this suppression was caused by IFN-γ produced by the CTLs themselves. These results suggest that strategies to regulate this treatment-induced recruitment of MDSCs could improve the efficacy of immunotherapy.

CTLs was compromised by massive accumulation of $CD11b^+Gr1^{int}Ly6C^+$ monocytic MDSCs in the tumor under the influence of the IFN-γ produced by the CTLs themselves.

Material and Methods

Mice, tumor cells and peptides

Male C57BL/6 mice at the age of 6 to 8 weeks were obtained from Japan SLC (Sizuoka, Japan) and used for dendritic cell (DC) preparation or as tumor-bearing mice in the ACT experiments. Mice transgenic for the Pmel-1-TCR recognizing the H-$2D^b$-restricted epitope EGSRNQDWL from gp100 (gp100 25-33) were obtained from The Jackson Laboratory (Bar Harbor, ME).[11] These mice are homozygous for the T lymphocyte-specific Thy1a (Thy1.1) allele. $CCR2^{-/-}$ mice were also purchased from The Jackson Laboratory and back-crossed for more than 10 generations onto the C57BL/6 background. All mice were housed in a pathogen-free environment.[13] All animal procedures were conducted in accordance with institutional guidelines. B16F10 is a gp100-positive spontaneous murine melanoma cell line, kindly provided by Dr. N. Restifo (National Cancer Institute) and maintained in culture medium consisting of DMEM (Wako Pure Chemical, Osaka, Japan) with 10% heat-inactivated fetal bovine serum (Bio West, Nuaillé, France), 100 μg/ml streptomycin and 100 U/ml penicillin (Wako Pure Chemical). The H-$2D^b$–restricted peptide human gp100 (hgp100 25–33, KVPRNQDWL) was purchased from GenScript Japan (Tokyo, Japan) at a purity of >90%, with a free amino terminal and carboxyl terminal.

DC preparation and CTL stimulation

DCs were obtained by 8-day culture of C57BL/6-derived bone marrow cells with granulocyte-macrophage colony stimulating factor (GM-CSF) as described previously.[14] Briefly, bone marrow cells obtained from tibias and femurs of C57BL/6 mice were cultured in RPMI 1640 medium supplemented with 10% FCS, 12.5 mM HEPES, 5×10^{-5} M 2-mercaptoethanol, 1×10^{-5} M sodium pyruvate, 1% nonessential amino acids, 100 U/ml penicillin, 100 μg/ml streptomycin and 20 ng/ml GM-CSF (PeproTech, Rocky Hill, NJ) for 8 days. On days 3 and 6, half the medium was replaced with fresh medium containing GM-CSF. DCs were further incubated with lipopolysaccharide (1 μg/ml) for 16 hr and then pulsed with hgp100 peptide (1 μg/ml) for 3 hr to obtain peptide-pulsed mature DCs. Spleen cells (1×10^7) from pmel-1-TCR transgenic mice were co-cultured with these DCs (2×10^5) for 3 days in medium containing 50 U/ml IL-2 (Chiron Corporation, Emeryville, CA) to prepare CTLs. After 3 days *in vitro* stimulation, approximately 90% of the harvested cells were $CD3^+CD8^+$ CTLs. Therefore, no further purification was performed before ACT.

ACT and anti-IFN-γ mAb treatment

C57BL/6 mice or $CCR2^{-/-}$ mice were first inoculated with 1×10^6 B16F10 cells subcutaneously on day 0, followed by adoptive CTL transfer (1×10^7) on day 9. Tumor growth was monitored every 2 to 3 days with calipers in a blinded fashion and was performed independently at least twice with similar results. On the day of, and 2 days after, CTL transfer, mice received intraperitoneal injections of 500 μg anti-IFN-γ mAb (clone XMG1.2, BioXCell, West Lebanon, NH) or rat IgG_1 isotype control (BioXCell). Tumor volume was calculated by the formula $\pi/6 \times L_1L_2H$, where L_1 is the long diameter, L_2 is the short diameter, and H is the height of the tumor. Survival was monitored periodically. Tumor-bearing mice either died or had to be euthanized when the tumor volume exceeded approximately 1,500 mm^3.

Cell preparation and flow cytometry

Tumors were harvested from mice at different time points, cut into pieces, and re-suspended in HBSS supplemented with 0.1% collagenase D (Roche Diagnostics, Indianapolis, IN) and DNase I (Roche Diagnostics) for 60 min at 37°C. The entire material was passed through a 70 μm cell strainer (BD Falcon, BD Bioscience) by being pressed with a plunger, to obtain single cell suspensions of tumor-infiltrating cells. For flow cytometry, these tumor digests were used without density gradient purification. The cells were first stained with Fixable Viability Dye eFluor450 (eBioscience, San Diego, CA) to label dead cells, and were pretreated with Fc Block (anti-CD16/32 clone 2.4G2; BD Pharmingen). The cells were then stained with antibodies and analyzed on a Gallios™ flow cytometer (Beckman Coulter, San Diego, CA). The following mAbs were obtained from BioLegend (San Diego, CA) and used for flow cytometry: FITC- or PerCP/Cy5.5-conjugated anti-CD45, PE-conjugated anti-NK1.1, Ly6G, PE/Cy7–conjugated anti-Ly6C, Alexa Fluor647-conjugated anti-CD90.1, APC-conjugated anti-CD107a, biotin-conjugated anti-Gr1, IL4Rα, F4/80, and Streptavidin-APC, APC-Cy7-conjugated anti-CD8, CD11b, Pacific Blue-conjugated anti-CD45. Data

were processed using Kaluza software (Beckman Coulter) and analyzed with FlowJo (version 7.6.5; TreeStar, Ashland, OR). The total numbers of cells were estimated from a FACS-based cell count of single cell suspensions. Flowcount beads (Beckman-Coulter, Galway, Ireland) were added to the cell samples and cell counts were calculated by the following equation: viable cells × total beads/counted beads.

Cell sorting was performed using a BD FACS Aria III (BD Bioscience). Single cell suspensions were centrifuged over the hypo-osmotic 1.10g/ml density solution OptiPrep (AXIS-SHIELD Poc AS, Oslo, Norway) and recovered from the interphase. Dead cells were excluded in flow cytometry on the basis of forward and side scatter profiles and Fixable Viability Dye eFluor450 (eBioscience). For the cytochemical and reverse transcription–polymerase chain reaction (RT-

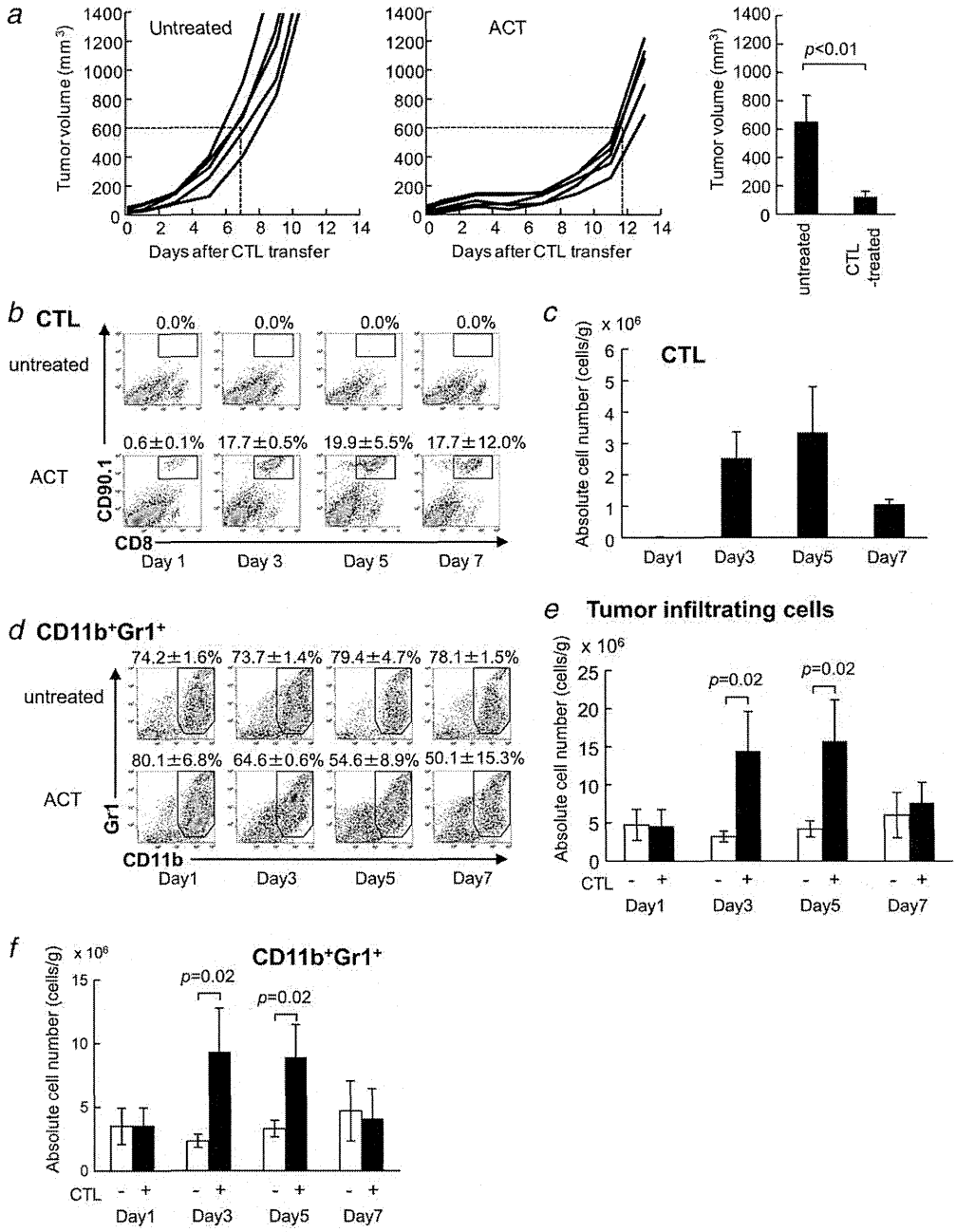

Figure 1.

PCR) analyses, $CD45^-$ tumor and stromal cells, $CD45^+CD11b^+Gr1^{high}Ly6C^{int}$ granulocytic MDSC, $CD45^+CD11b^+Gr\text{-}1^{int/dull}Ly6C^+$ monocytic MDSC, and $CD11b^+Gr\text{-}1^{int/low}Ly6C^-$ macrophage were sorted.

The CD107a externalization assay

To evaluate the cytotoxic function of CTLs, cells (5×10^5) were stimulated for 4 hr with 1 μg/ml mgp100 peptide and 0.5 μl of APC-conjugated anti-CD107a antibody (Biolegend) or isotype control (Rat IgG2a, κ, Biolegend).[15] Cells were stained with Pacific Blue-conjugated anti-CD45, APC-Cy7-conjugated CD8, FITC-conjugated CD90.1. $CD45^+CD8^+CD90.1^+$ cells were gated and CD107a expression was determined as an indicator of degranulation.

ROS production

To detect the production of reactive oxygen species (ROS) from monocytic MDSC, cells were stained with 0.6 μM 5-(and-6)-chloromethyl-2',7'-dichlorodihydrofluorescein diacetate, acetyl ester (CM-H_2DCFDA, Invitrogen) for 30 min at 37°C.[16] Cells were stained with PerCP/Cy5.5-conjugated anti-CD45, APC-Cy7-conjugated anti-CD11b, APC-conjugated anti-Gr1, PE-Cy7-conjugated anti-Ly6C and Fixable Viability Dye eFluor450 (eBioscience, San Diego, CA). $eFluor450^-CD45^+CD11b^+Gr1^{int}Ly6C^+$ cells were gated and ROS production was assessed by the green fluorescence intensity of CM-H_2DCFDA.

CFSE labeling and proliferation assay

To prepare responder cells, splenocytes were harvested from pmel-1 TCR-transgenic mice and $CD8^+$ cells were magnetically enriched by positive selection using a magnetic cell sorting system (Miltenyi Biotec, Bergisch Gladbach, Germany). $CD8^+$ pmel-1 cells were washed twice with PBS and resuspended at 10^7 cells/ml in PBS/1% BSA, 0.6 μM carboxyfluorescein diacetate succinimidyl ester (CFSE, Invitrogen) for 10 min at 37°C. The labeling was stopped by washing twice with cold RPMI with 10% FCS. To prepare inhibitor cells, monocytic MDSCs were enriched from tumor infiltrating cells on day 3 after CTL transfer. Cells were centrifuged over the hypo-osmotic 1.077g/ml density solution OptiPrep (AXIS-SHIELD Poc AS) and cells recovered from the interphase. This procedure eliminates dead cells and granulocytes, including granulocytic MDSC. $CD11b^+$ cells were then isolated using EasySep Mouse CD11b Positive Selection Kits (STEMCELL Technologies, Vancouver, BC) according to the manufacturer's instructions. The purity of monocytic MDSC was routinely >90%. CFSE-labeled pmel-1 cells (5×10^5) were then stimulated for 72 hr in 96-well flat-bottom plates (Greiner Japan, Tokyo, Japan) with hgp100 peptide (1 μg/ml). To assess the immunosuppressive activity of MDSCs, 1.5, 5.0 or 15×10^5 MDSC were added to the cultures. On day 3 of the assay, cells were harvested and stained with PE-labeled anti-CD8 and Alexa 647-labeled anti-Thy1.1 (CD90.1, Biolegend). A total of 100,000 events were collected for each sample by flow cytometry; $CD8^+CD90.1^+$ cells were gated and fluorescence intensity of CFSE was evaluated. The assays were also performed in the presence of 0.5 mM NG-monomethyl-L-arginine (L-NMMA) (inducible nitric oxide synthase (iNOS) inhibitor, Dojindo, Kumamoto, Japan), 10 mM N-acetyl-l-cysteine (ROS inhibitor, Sigma, Saint Louis, MO) and 0.5 mM Nω-hydroxy-nor-l-arginine (Nor-NOHA) (arginase I inhibitor, Calbiochem, San Diego, CA).

Quantitative real-time polymerase chain reaction

Total RNA was extracted using TRIZOL according to the manufacturer's instructions (Invitrogen, Carlsbad, CA). The purity and RNA concentration was determined using a NanoDrop spectrophotometer (Thermo Scientific, Wilmington, DE). The RNA was converted to cDNA using the SuperScript III First-Strand Synthesis System according to the manufacturer's instructions (Invitrogen, Carlsbad, CA), and qRT-PCR reactions were carried out using EXPRESS SYBR GreenER qPCR SuperMix Universal (Invitrogen). Primer sequences are given in Supporting Information Table S1. The PCR reactions were run in a Thermal Cycler Dice Real Time System TP800 (Takara, Shiga, Japan) using the following program: 1 cycle of 95°C for 2 min, 40 cycles

Figure 1. Infiltration of adoptively-transferred CTLs into the tumor induces massive accumulation of other cell types. (*a*) Adoptive CTL transfer (ACT) suppresses tumor growth. B16 melanoma cells (1×10^6) were implanted subcutaneously in 6-week-old C57BL/6 mice (five mice per group). Tumor growth was measured in mice bearing 9-d B16 tumors that received *in vitro* activated pmel-1 splenocytes (1×10^7) as CTLs. Tumor volume was calculated by the formula $\pi/6 \times L_1L_2H$, where L_1 is the long diameter, L_2 is the short diameter, and H is the height of the tumor. (*b*) Infiltration of tumor-specific CTLs into the tumor was analyzed. Mice ($n = 3$) were killed at the indicated time points and mononuclear cells were isolated from the tumor. In brief, tumors were cut into pieces, and digested in HBSS supplemented with 0.1% collagenase D (Roche Diagnostics, Indianapolis, IN) and DNase I (Roche Diagnostics) for 60 min at 37°C. The entire material was passed through a 70 μm cell strainer (BD Falcon, BD Bioscience) by being pressed with a plunger, to obtain single cell suspensions of tumor-infiltrating cells. For flow cytometry, these tumor digests were used without density gradient purification. Cells were stained with Fixable Viability Dye eFluor450 to label dead cells. Then, $CD45^+$ cells were gated to discriminate immune cells form tumor cells. The frequency of CTL at the tumor site was analyzed as $eFluor450^-CD45^+CD8^+CD90.1^+$ and the absolute number of CTLs was calculated (*c*). (*d*) $eFluor450^-CD45^+$ cells were further stained with anti-CD11b and -Gr1 mAbs to detect MDSCs. The absolute number of tumor infiltrating cells (*e*) and $CD11b^+Gr1^+$ cells (*f*) at the indicated time points were shown. Numbers of each population were calculated as described in the Materials and Methods section and adjusted by the tumor weight (cells/g). □ untreated mice, ■ ACT mice. Numbers on the images show the percentage of CD45 gated cells (mean ± SD). All experiments shown were performed independently at least three times with similar results.

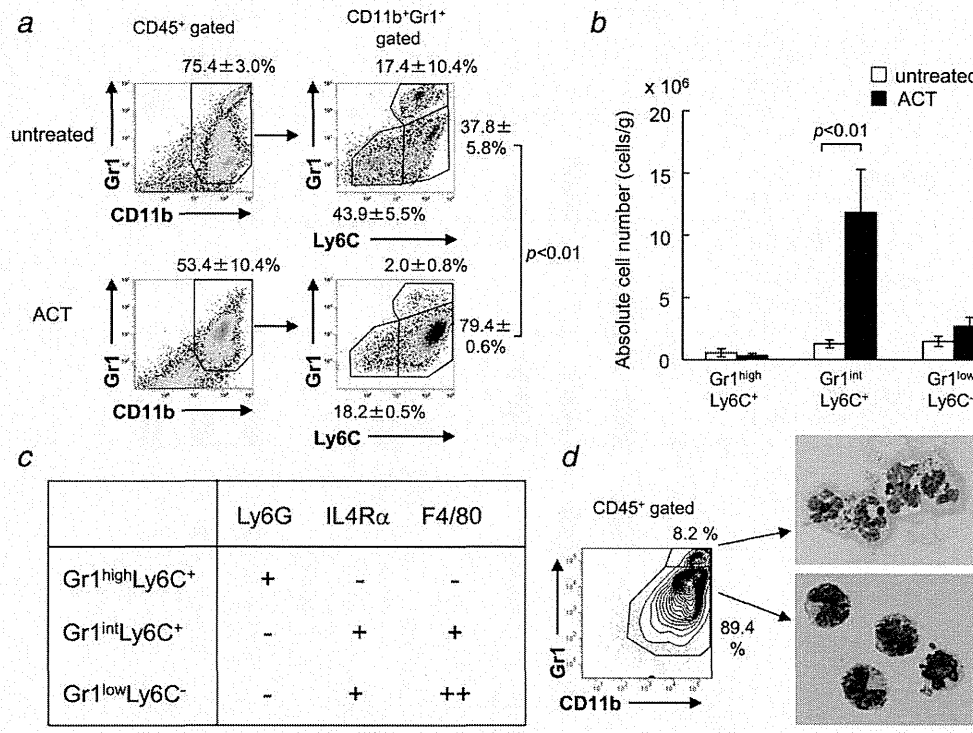

Figure 2. The characteristic phenotype of CTL-induced MDSCs. Tumor-bearing mice (n = 4) were treated as described in Figure 1. Tumor–infiltrating cells were harvested 3 days after ACT and analyzed by flow cytometry. (*a*) eFluor450$^-$CD45$^+$CD11b$^+$Gr1$^+$ cells were further defined by the expression of Ly6C. Numbers on the top of the images show the percentage of gated cells (mean ± SD). (*b*) Numbers of Gr1^{high}Ly6C$^+$, Gr1^{int}Ly6C$^+$ and Gr1^{low}Ly6C$^-$ cells were compared w/o ACT. □ untreated mice, ■ ACT mice. (*c*) Surface phenotypes of MDSCs were further defined by the expression of Ly6G, IL-4Rα and F4/80. (*d*) CD11b$^+$Gr1^{high} and CD11b$^+$Gr1^{int}cells were sorted from day 3 infiltrates from ACT mice (n = 5), stained with Diff quick as described in Materials and Methods; their morphology was assessed using an OLYMPUS BX41 microscope. All experiments shown were performed independently at least three times with similar results. [Color figure can be viewed in the online issue, which is available at wileyonlinelibrary.com.]

95°C for 15 sec, 60°C for 30 sec. Results are expressed as ratios. The quantity of target mRNA was normalized to the level of GAPDH in each sample. PCR was performed in duplicate for each experiment and the PCR products were also monitored by electrophoresis on 1.8% agarose gels and visualized with ethidium bromide.

Cytology

Smears were prepared from each sorted cell population, air dried, and stained with Diff quick (Sysmex, Kobe, Japan) according to the manufacturer's instructions. Cell morphology was evaluated using bright field microscopy (OLYMPUS BX41 with Canon EOS Kiss X4 digital camera, OLYMPUS, Tokyo, Japan, magnification 1,000×).

Histologic analysis

Fresh frozen sections were stained as described previously.[17] In brief, cryosections were fixed in ice-cold acetone and preincubated in Block Ace (Dainippon Pharmaceutical, Tokyo, Japan). Subsequently, samples were incubated with primary antibodies or appropriate control antibodies, followed by appropriate Alexa Fluor-labeled secondary reagents (Invitrogen Japan K.K., Tokyo, Japan). The samples were then analyzed using BZ-9000 fluorescence microscope with BZ-II image processing software (KEYENCE, Osaka, Japan). Purified anti-mouse F4/80, FITC-conjugated Ly6C, APC-conjugated CD90.1, anti-APC-biotin were purchased from Biolegend. Goat anti-Rat IgG-Alexa 546, Rabbit anti-FITC Alexa 488, Donkey anti-Rabbit 488, Streptavidin-Alexa 647 were purchased from Invitrogen. Tissues were also fixed in 10% neutral formalin (Muto Pure Chemicals, Tokyo, Japan), embedded in paraffin, sectioned (3 mm), and stained with hematoxylin and eosin.

Statistical analysis

Statistical analyses were performed with JMP software, version 9.0.0. (SAS Institute Inc., Cary, NC). Results are shown as mean ± SD. Comparison of results was carried out using the two-tailed unpaired t-test.

Results

Adoptively-transferred CTLs migrate to the tumor and induce accumulation of myeloid cells

To investigate the mechanisms responsible for effective immunotherapy, we utilized a murine model with B16

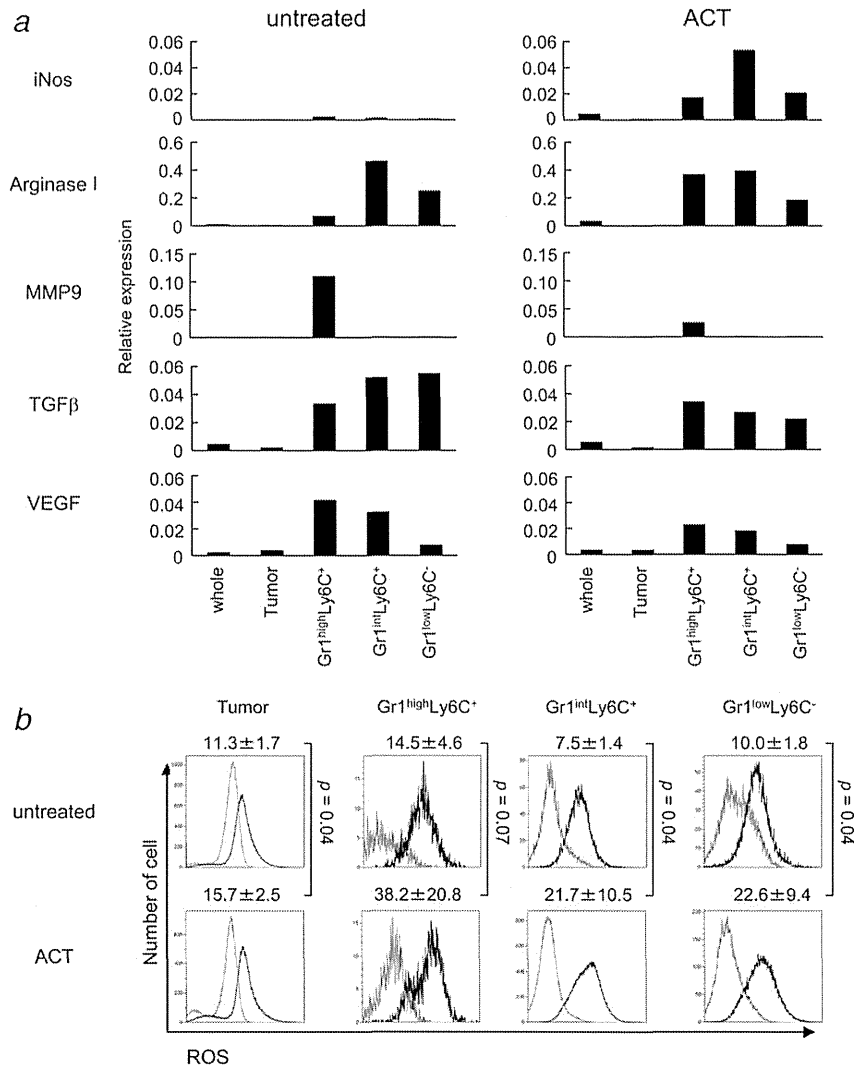

Figure 3. Immunosuppressive effector molecules of MDSCs. (*a*) Tumor-bearing mice ($n = 3$) were treated as described in Figure 1. Tumor-infiltrating cells were harvested 3 days after CTL transfer, pooled and stained with eFluor450, ant-CD45-FITC, anti-CD11b-APC/Cy7, anti-Gr1-APC and anti-Ly6C-PE/Cy7. $CD45^-$ tumor cells, $Gr1^{high}Ly6C^+$ granulocytic MDSC, $Gr1^{int}Ly6C^+$ monocytic MDSC and $Gr1^{low}Ly6C^-$ cells were sorted and mRNA was isolated. The messages for iNOS, arginase I, MMP9, TGFβ and VEGF were analyzed by quantitative RT-PCR. (*b*) Tumor-infiltrating cells were stained with anti-CD45-PerCP/Cy5.5, anti-CD11b-APC/Cy7, anti-Gr1-APC, anti-Ly6C-PE/Cy7 and CM-H_2DCFDA; ROS expression was compared with the green fluorescence intensity. Numbers on the top of the images show the fluorescent intensity (mean ± SD). All experiments shown were performed independently at least three times with similar results.

melanoma cells and pmel-1-TCR transgenic T cells. As shown in Figure 1*a*, tumors grew progressively in untreated mice. In contrast, tumor growth was suppressed in mice receiving CTLs by adoptive transfer. On day 7, the tumor volume in untreated and CTL-treated (designated as ACT) animals was 654.9 ± 185.4 mm^3 and 122.6 ± 40.5 mm^3, respectively ($p < 0.01$). While tumors exceeded 600 mm^3 by day 6.8 ± 0.9 in untreated mice, this took 11.7 ± 0.5 days in ACT mice ($p < 0.01$). These results indicate that adoptively-transferred CTLs cause a significant delay in tumor growth. However, anti-tumor activity was transient and tumors started to grow again around day 8.

To investigate the underlying mechanisms that limit the duration of anti-tumor activity of these infused CTLs, dynamic changes in the cells present within the tumor were analyzed. Tumors were isolated from untreated or ACT mice at the indicated time points after CTL transfer and were examined by histology with standard hematoxylin-eosin staining (Supporting Information Fig. S1). Only scattered inflammatory infiltrates were observed in the tumor from untreated mice and ACT mice on day 1. Massive infiltration of mononuclear cells and destruction of tumor cells were observed on day 3 and 5 after CTL transfer. The inflammatory response slightly subsided on day 7. To further investigate the tumor infiltrating cells, mice

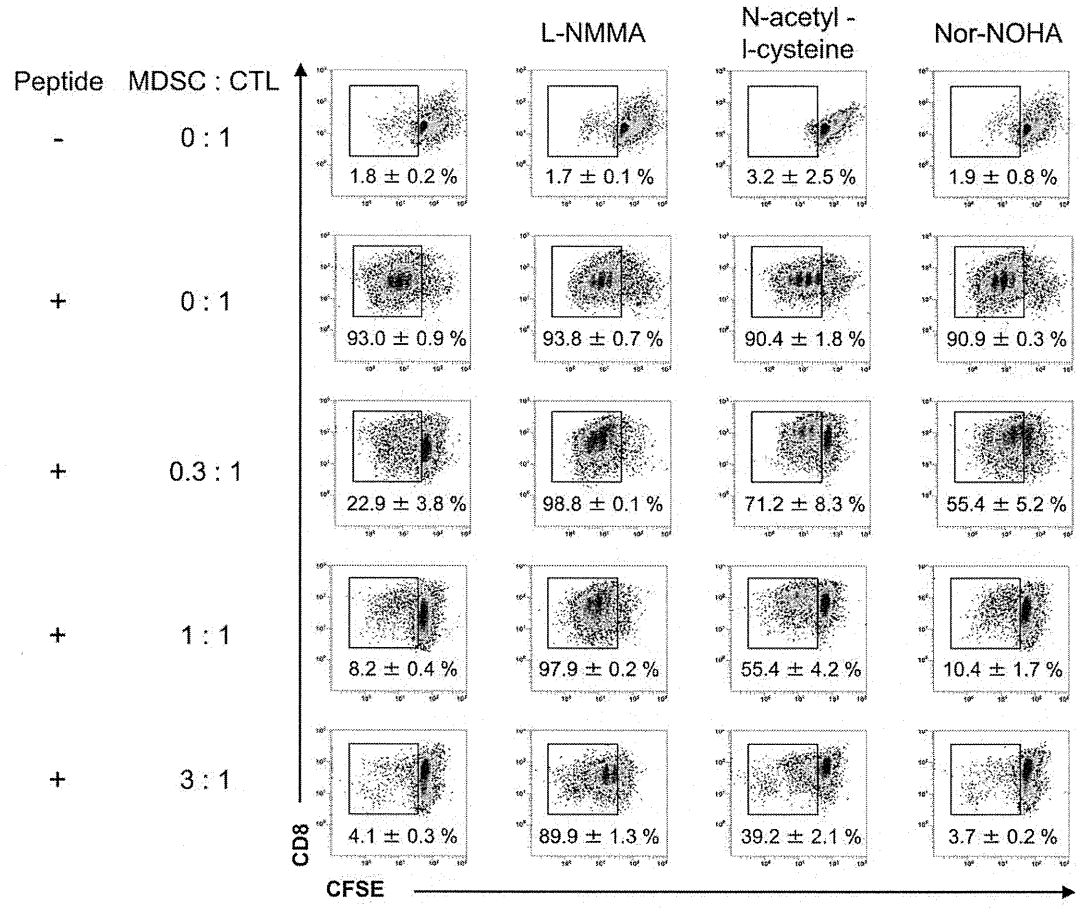

Figure 4. MDSCs inhibit the proliferation of antigen-specific CTLs. Tumor-bearing mice (n = 10) were treated as described in Figure 1. Tumor-infiltrating cells were harvested from B16 tumor 3 days after CTL transfer and MDSCs were positively selected by anti-CD11b magnetic beads. CFSE-labeled pmel-1 cells were stimulated with hgp100 peptide in the presence or absence of MDSCs at the indicated ratio. The proliferation of pmel-1 cells was evaluated by flow cytometry. The proliferation of pmel-1 cells was further studied in the presence of L-NMMA (iNOS inhibitor), *N*-acetyl-L-cysteine (ROS inhibitor) and Nor-NOHA (arginase I inhibitor). Numbers on the images show the percentage of gated cells (mean ± SD). All experiments shown were performed independently at least three times with similar results.

were sacrificed at different time points after infusing CTLs and mononuclear cells were isolated from their tumors. The cells were stained with eFluor450 to label dead cells and the percentages and numbers of eFluor450$^-$CD45$^+$ cells were analyzed by flow cytometry (Fig. 1). Adoptively-transferred CTLs preferentially infiltrated into the tumor. In ACT mice, CD8$^+$CD90.1$^+$ CTLs were detected in the tumor as early as day 1 after CTL transfer, peaked on day 3 to 5 and gradually decreased by day 7 (Figs. 1*b* and 1*c*). The presence of CTLs in the tumor paralleled the inhibition of tumor growth observed in these ACT mice.

In untreated mice on day 1, the percentages of CD8$^+$, CD4$^+$ and NK1.1$^+$ cells in the tumor were approximately 3.8 ± 2.1%, 5.3 ± 1.3% and 3.2 ± 1.4%, respectively (Supporting Information Fig. S2). The percentage of CD11b$^+$Gr1$^+$ cells was 74.2 ± 1.6% (Fig. 1*d*). Thus, the majority of tumor-infiltrating cells were not lymphocytes but consisted of CD11b$^+$Gr1$^+$ myeloid cells. In ACT mice, the tumor-infiltrating CTLs were accompanied by massive accumulation of other cells (Fig. 1*e*). While about 5.0 × 10^6 cells per gram tumor weight were harvested from B16 tumors in untreated mice, we obtained 1.4 ± 0.5 × 10^7 and 1.6 ± 0.5 × 10^7 from ACT mice on day 3 and 5, respectively (Fig. 1*e*). CTL transfer did not affect the frequency of recipient-derived CD8$^+$ (eFluor450$^-$CD45$^+$CD8$^+$CD90.1$^-$) and CD4$^+$ T cells (Supporting Information Figs. S2A and B). However, the absolute numbers of these cells were increased. The frequency and number of NK cells (eFluor450$^-$CD45$^+$NK1.1$^+$) in the tumor slowly increased after CTL transfer (Supporting Information Fig. S2C). Of note, massive accumulation of CD11b$^+$Gr1$^+$ cells was observed in the tumor (Figs. 1*d* and 1*f*). This was not reflected in an increased percentage of CD11b$^+$Gr1$^+$ cells in the tumor relative to the untreated animals, but the absolute number of these cells in ACT mice was much greater (p = 0.02) (Fig. 1*f*). The numbers of CD11b$^+$Gr1$^+$ cells in ACT mice were 3.6 ± 1.4 × 10^6, 9.3 ± 3.4 × 10^6, 8.9 ± 2.2 × 10^6,

and 4.1 ± 2.3 × 10^6 on days 1, 3, 5, and 7, respectively (Fig. 1*f*). ACT induced massive recruitment of $CD11b^+Gr1^+$ cells in the tumor with similar kinetics to the CTLs.

Increased infiltrating myeloid cells after ACT is characterized as $Gr1^{int}Ly6C^+$ monocytic MDSC

Tumor-infiltrating cells were harvested from ACT and untreated mice on day 3 after CTL transfer; $CD11b^+Gr1^+$ cells were gated and further analyzed by anti-Ly6C mAb. They were divided into three populations, $Gr1^{high}Ly6C^+$, $Gr1^{int}Ly6C^+$ and $Gr1^{low}Ly6C^-$ cells (Fig. 2*a*). As shown in Figure 2*a*, the $Gr1^{int}Ly6C^+$ cell population was increased from 37.8 ± 5.8% in untreated mice to 79.4 ± 0.6% in ACT mice. The absolute number of $Gr1^{int}Ly6C^+$ cells in ACT mice was 9.2-fold that of control mice (1.2 ± 0.3 × 10^7 *vs.* 1.3 ± 0.3 × 10^6) (Fig. 2*b*). In contrast, the percentage of $Gr1^{high}Ly6C^+$ in ACT mice was decreased to 2.0 ± 0.8% compared with 17.4 ± 10.4% in controls (Fig. 2*a*), although their absolute number was not different (Fig. 2*b*). Because it is known that the Gr1 mAb binds to both Ly6G and Ly6C molecules, we further defined these cells by anti-Ly6G and Ly6C mAbs separately. We found that Ly6G was expressed by $CD11b^+Gr1^{high}Ly6C^+$ cells, but not $CD11b^+$ $Gr1^{int}Ly6C^+$ cells. IL4Rα and F4/80 were expressed by both $Gr1^{int}Ly6C^+$ and $Gr1^{low}Ly6C^-$ populations (Fig. 2*c*). These data show that $CD11b^+Gr1^{high}Ly6G^+Ly6C^+$ granulocytic MDSC, $CD11b^+Gr1^{int}Ly6G^-Ly6C^+$ monocytic MDSC and $CD11b^+Gr1^{low}Ly6G^-Ly6C^-F4/80^{++}$ macrophage were present in the B16 tumors. The cells preferentially accumulating in the tumor following ACT were therefore monocytic MDSC. Accordingly, $CD11b^+Gr1^{high}$ and $CD11b^+Gr1^{int}$cells were sorted from day 3 infiltrating cells from ACT mice and their morphology examined by light microscopy (Fig. 2*d*). Multilobed or polymorph nuclei were observed in $CD11b^+Gr1^{high}$ cells and eccentrically-placed kidney bean-shaped nuclei in $CD11b^+Gr1^{int}$ cells. Consistent with these single cell analysis, infiltration of adoptively-transferred CTLs and recruitment of monocytic MDSCs were observed in the tumor after ACT by immunohistochemistry (Supporting Information Fig. S3). While only a few $CD90.1^+$ CTLs (blue) were detected in the tumor on day1, diffuse infiltration of CTLs were observed in the tumor on day 3 to 7. Infiltration of CTLs were accompanied by 3-5 times more in number of the recruitment of $Ly6C^+$ monocytic MDSCs (green). The distribution of $CD90.1^+$ CTLs, $Ly6C^+$ monocytic MDSCs, and $F4/80^+$ macrophages were compared between the center and the peripery of the tumor on day 3 (Supporting Information Fig.S4). CTLs and macropahges distributed throughout the tumor tissue in a disseminated manner as scattered solitary cells. Aggregates and condensations of monocytic MDSC co-localized with CTLs. These results suggested that tumor infiltrating CTLs recruited monocytic MDSC.

Adoptively-transferred CTLs activate monocytic MDSC

It has been reported that granulocytic MDSC use ROS to mediate suppression,[18] whereas monocytic MDSC use upregulation of NO and arginase.[19] To determine whether cells accumulating in the tumors of ACT mice have such suppressive functions, we assessed the expression of these suppressive molecules by cells isolated from the tumor 3 days after CTL transfer (Fig. 3*a*). First, CD45 expression was used to separate leukocytes from tumor cells. Next, granulocytic MDSC and monocytic MDSC were isolated according to their Gr1 and Ly6C expression as defined in Figure 2*a*. Quantitative RT-PCR was performed with mRNA extracted from tumor cells and leukocytes isolated from ACT and untreated mice. mRNAs for iNOS, arginase I, MMP9, TGFβ, and VEGF were detected in leukocytes from both untreated and ACT mice. Although MMP9, TGFβ, and VEGF were decreased in the ACT mice, iNOS was markedly upregulated in the $Gr1^{int}Ly6C^+$ monocytic MDSCs from these animals. Furthermore, cells were isolated and stained with the mAbs and with CM-H_2DCFDA, an indicator for the production of ROS. As shown in Figure 3*b*, monocytic MDSC from both ACT and control mice produced ROS, but the fluorescence intensity of the former was enhanced relative to the latter (p = 0.04). These results indicate that monocytic MDSC expressed immunosuppressive molecules and that CTL treatment was accompanied by an upregulation of these immunosuppressive molecules in MDSC.

Monocytic MDSC suppress CTL proliferation

The capacity of MDSC to suppress antigen-specific T-cell proliferation was investigated, with the results shown in Figure 4. MDSCs were harvested from B16 tumor 3 days after CTL transfer and positively selected by anti-CD11b magnetic beads. Their purity was 91.6% (data not shown). To prepare responder cells, gp100-specific T cells were isolated from pmel-1 TCR transgenic mice (designated pmel-1 cells) and labeled with CFSE. MDSCs were pulsed with 1 μg/ml hgp100 peptide and co-cultured with CFSE-labeled pmel-1 cells for 3 days. Pmel-1 spleen cells did not proliferate without peptide (Fig. 4, upper left). In the presence of peptide and without MDSCs, 93.0 ± 0.9% of pmel-1 cells experienced cell division within 3 days. When MDSCs were added to the cultures, proliferation was inhibited in a dose-dependent manner. When MDSCs were incubated with pmel-1 cells at a ratio of 0.3:1, 1:1 or 3:1, 22.9 ± 3.8%, 8.2 ± 0.4%, 4.1 ± 0.3% of pmel-1 cells divided, respectively. These results indicate that MDSCs in the tumors of ACT mice inhibited the proliferation of the infused antigen-specific CTLs.

To identify the factors responsible for the immunosuppressive activity of these MDSC, blockade of pmel-1 cell proliferation was tested in the presence of L-NMMA (iNOS inhibitor), *N*-acetyl-L-cysteine (ROS inhibitor) or Nor-NOHA (arginase I inhibitor). By themselves, these reagents had no effect on pmel-1 proliferation at the concentrations used (Fig. 4, upper two lanes). However, in the presence of L-NMMA, inhibition of pmel-1 proliferation by MDSC was completely abrogated. Even when three times more MDSCs were added to the culture, 89.9 ± 1.3% of pmel-1 cells still proliferated.

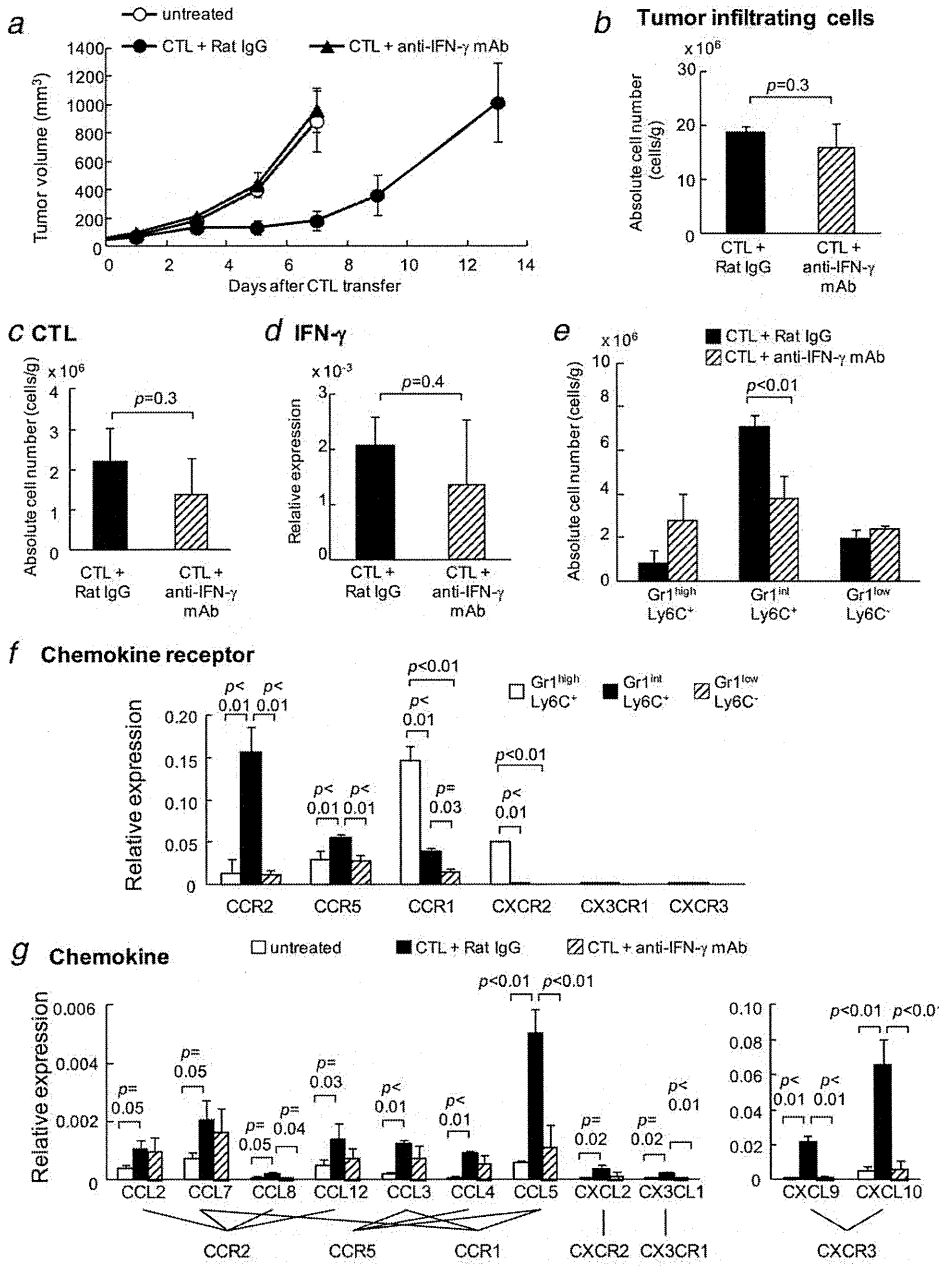

Figure 5. The anti-tumor activity of CTLs and the accumulation of monocytic MDSCs is mediated by IFN-γ. B16 melanoma cells (1×10^6) were implanted subcutaneously in 6-week-old C57BL/6 mice (six or seven mice per group). Tumor growth was measured in mice bearing 9-d B16 tumors that received 1×10^7 CTLs activated *in vitro*. ACT mice were divided into two groups; one received anti-IFN-γ mAb and the other received control Rat IgG_1. (*a*) Tumor volume was compared between untreated and ACT mice w/o anti-IFN-γ mAb treatment. Tumor-infiltrating cells were harvested 3 days after ACT. The number of tumor-infiltrating cells (*b*) and CTLs (*c*) and intratumoral expression of IFN-γ mRNA (*d*) were compared between IFN-γ-treated or control IgG-treated mice after ACT. (*e*) The number of $Gr1^{high}Ly6C^+$ granulocytic MDSC, $Gr1^{int}Ly6C^+$ monocytic MDSC and $Gr1^{low}Ly6C^-$ cells were also compared. ■ CTL + Rat IgG-treated mice, ▨ CTL + anti-IFN-γ mAb-treated mice. (*f*) $Gr1^{high}Ly6C^+$ granulocytic MDSC, $Gr1^{int}Ly6C^+$ monocytic MDSC and $Gr1^{low}Ly6C^-$ cells were sorted from ACT mice without anti-IFN-γ mAb 3 days after CTL transfer and RNA was isolated. The messages for chemokine receptors, CCR2, CCR5, CCR1, CXCR2, CX3CR1 and CXCR3, were compared in these cell populations (□ $Gr1^{high}Ly6C^+$, ■ $Gr1^{int}Ly6C^+$, ▨ $Gr1^{low}Ly6C^-$ cells) by quantitative RT-PCR. (*g*) Tumors were harvested on day 3 after CTL transfer and total RNA was isolated. The mRNA expression of chemokines, CCL2, CCL7, CCL8, CCL12, CCL3, CCL4, CCL5, CXCL2, CX3CL1, CXCL9 and CXCL10, were compared with these animals (□ untreated, ■ CTL + Rat IgG-treated mice, ▨ CTL + anti-IFN-γ mAb-treated mice) by qRT-PCR. All experiments shown were performed independently at least three times with similar results.

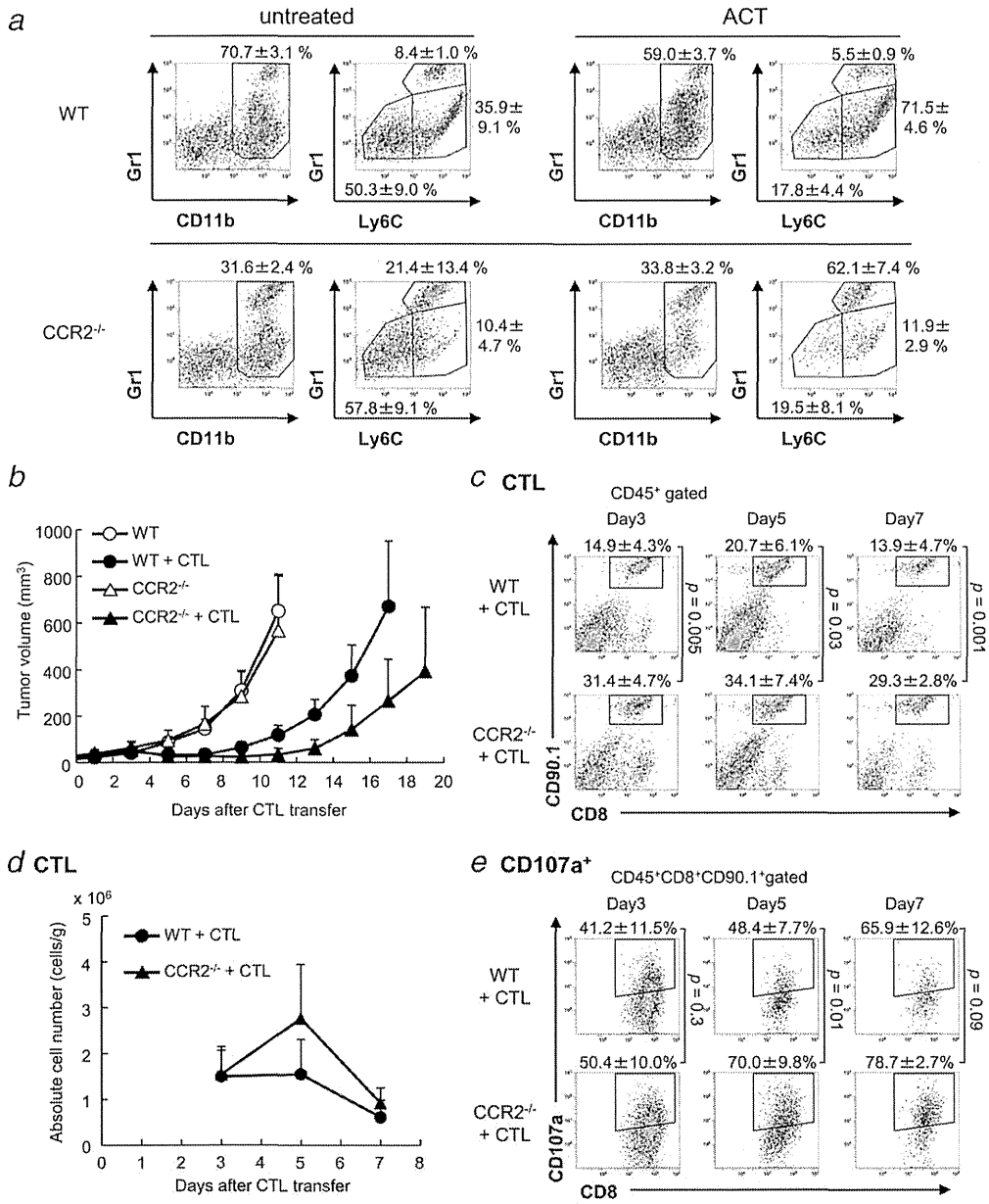

Figure 6. CTL-induced anti-tumor activity and MDSC accumulation in CCR2$^{-/-}$ mice. B16 melanoma cells (1 × 10^6) were implanted subcutaneously in 6-week-old C57BL/6 mice (WT) or CCR2$^{-/-}$ mice. On day 9, tumor-bearing mice (n = 4) received 1 × 10^7 CTLs. A, Tumor-infiltrating cells were harvested 3 days after CTL transfer and MDSCs were compared with WT and CCR2$^{-/-}$ mice. (*b*) Tumor growth was measured in mice (five to seven mice per group) bearing 9-d B16 tumors w/o 1 × 10^7 CTL transfer. Suppression of tumor growth by CTLs is augmented in CCR2$^{-/-}$ mice. (*c*) Tumor-infiltrating cells were harvested on day 3, 5, and 7. Cells were gated on CD45$^+$; the infiltration of CTLs into the tumor was compared between WT and CCR2$^{-/-}$ mice. (*d*) The absolute number of CTLs on days 3, 5 and 7 after ACT in WT and CCR2$^{-/-}$ mice. (*e*) Tumor-infiltrating cells were harvested at the indicated time points and stimulated with 1 μg/ml mgp100 peptide. Cells were gated on CD45$^+$CD8$^+$CD90.1$^+$; Externalization of CD107a on CD8$^+$CD90.1$^+$ CTLs was evaluated. Numbers on the images show the percentage of gated cells (mean ± SD). All experiments shown were performed independently at least three times with similar results.

Suppression of pmel-1 proliferation was also diminished by *N*-acetyl-L-cysteine; it was restored to 39.2 ± 2.1% from 4.1 ± 0.3% at an MDSC:CTL ratio of 3:1. Finally, although Nor-NOHA did not restore pmel-1 proliferation at the MDSC:CTL ratio of 3:1, it was slightly increased from 22.9 ± 3.8% to 55.4 ± 5.2% at a ratio of 0.3:1. These results indicate that NO, ROS and Arginase I are all involved in the immunosuppressive activity of MDSCs after ACT.

Both tumor growth suppression and stimulation of monocytic MDSCs by adoptively transferred CTLs is mediated by IFN-γ

To determine the factors responsible for the activation of MDSCs, anti-IFN-γ neutralizing mAb was administered intraperitoneally to ACT mice. On the day of, and 2 days after, CTL transfer, mice received either 500 μg anti-IFN-γ mAb or rat IgG_1 isotype control. Treatment with anti-IFN-γ mAb was found to completely abrogate the anti-tumor activity of transferred CTLs (Fig. 5*a*). Thus, even though mice received CTLs, tumors in anti-IFN-γ mAb-treated mice grew progressively with the same kinetics as in untreated mice. Tumor-infiltrating cells were harvested 3 days after ACT in animals treated or not treated with anti-IFN-γ mAb. The absolute number of tumor infiltrating cells was comparable between these two groups (Fig. 5*b*). The degree of CTL infiltration into the tumor, as well as the level of intra-tumoral IFN-γ expression was the same in anti-IFN-γ mAb-treated and isotype control-treated mice, although slightly but non-significantly reduced in the former (Figs. 5*c* and 5*d*). Nonetheless, the anti-tumor activity of the CTLs was completely abrogated in the anti-IFN-γ mAb-treated mice. The percentage and number of $Gr1^{int}Ly6C^{+}$ monocytic MDSC in the tumor were both decreased by neutralization of IFN-γ although the overall number of tumor infiltrating cells remained the same (Figs. 5*b* and 5*e*). These results indicate that both tumor growth suppression and expansion of monocytic MDSC in the tumor depend on the IFN-γ produced by the tumor-specific CTLs.

The anti-tumor activity of the CTLs is augmented in the absence of monocytic MDSC

To determine the factors responsible for the recruitment of MDSCs into the tumor, mRNA expression of chemokine receptors was compared on $Gr1^{high}Ly6C^{+}$, $Gr1^{int}Ly6C^{+}$ and $Gr1^{low}Ly6C^{-}$ cells after ACT (Fig. 5*f*). While $Gr1^{high}Ly6C^{+}$ granulocytic MDSCs express CCR1, $Gr1^{int}Ly6C^{+}$ monocytic MDSCs expressed CCR2. Consistently, CCR2 ligands, CCL2, CCL7 and CCL12 were expressed in the tumor and up-regulated by ACT (Fig. 5*g*). The up-regulation of CCL7 and CCL12 expression was diminished by anti-IFN-γ treatment. These results suggested that CCR2 axis was involved in the recruitment of monocytic MDSCs into the tumor by ACT.

Therefore, we compared the anti-tumor activity of adoptively-transferred CTLs in $CCR2^{-/-}$ mice. B16 tumor cells were subcutaneously inoculated into C57BL/6 wild-type and $CCR2^{-/-}$ mice. Consistent with our previous report,[20] we found that the $CD11b^{+}Gr1^{int}Ly6C^{+}$ monocytic MDSCs decreased in tumor-infiltrating cells from $CCR2^{-/-}$ mice. However, $CD11b^{+}Gr1^{high}Ly6C^{+}$ granulocytic MDSC were increased from 8.4 ± 1.0% to 21.4 ± 13.4% (Fig. 6*a*). CTLs were then adoptively transferred and tumor-infiltrating cells harvested on day 3. CTLs in the tumor in wild-type mice were accompanied by the accumulation of $CD11b^{+}Gr1^{+}$ cells, especially $Ly6C^{+}$ monocytic MDSC. In contrast, $CD11b^{+}Gr1^{int}Ly6C^{+}$ monocytic MDSC were not present in CTL-treated $CCR2^{-/-}$ mice, which instead accumulated granulocytic MDSC. While 71.5 ± 4.6% of infiltrating cells were monocytic MDSC in wild-type mice, this was only 11.9 ± 2.9% in $CCR2^{-/-}$ mice, which had 62.1 ± 7.4% of granulocytic MDSC (Fig. 6*a*).

As shown in Figure 6*b*, tumors grew progressively not only in wild-type mice, but in $CCR2^{-/-}$ mice as well. As expected, tumor growth was suppressed in mice receiving CTLs by adoptive transfer, and more effectively in the absence of CCR2. These results indicate that the anti-tumor activity of transferred CTLs was augmented in the absence of monocytic MDSC accumulation. To investigate the underlying mechanisms for this, tumor-infiltrating cells were harvested and infiltration of CTLs compared at the indicated time points. The percentages of CTLs in infiltrating cells from wild-type mice at days 3, 5 and 7 were 14.9 ± 4.3%, 20.7 ± 6.1% and 13.9 ± 4.7%, respectively (Fig. 6*c*). In CTL-treated $CCR2^{-/-}$ mice, the infiltration of CTLs into the tumor was increased at days 3, 5 and 7 to 31.4 ± 4.7%, 34.1 ± 7.4% and 29.3 ± 2.8%, respectively. The absolute number of CTLs in the tumor was 3.0 ± 1.4 × 10^6 in $CCR2^{-/-}$ mice compared with 1.7 ± 0.8 × 10^6 in wild-type mice on day 5 after CTL transfer (Fig. 6*d*). More $CD107a^{+}$ CTLs were present in the tumor of $CCR2^{-/-}$ mice receiving CTLs (Fig. 6*e*). These results indicated that more CTLs infiltrated into the tumor and exerted better effector function in the absence of monocytic MDSC recruitment.

Discussion

Established tumors comprise multiple cellular constituents.[21] Complex interactions between the different cell types in the tumor contribute to the immunosuppressive microenvironment. Here, we examine the effect of ACT on this complex regulatory network in the tumor. Adoptively-transferred CTLs that infiltrated into the tumor and exerted anti-tumor activity were associated with a massive recruitment of other leukocytes (Supporting Information Fig. S1), the majority of which was a $CD11b^{+}Gr1^{int}Ly6G^{-}Ly6C^{+}$ monocytic MDSC population (Figs. 1, 2 and Supporting Information Fig. S3). This resulted in increased immunosuppressive activity in the tumor microenvironment and suppressed the CTLs, forming a negative feedback loop.

MDSCs were originally identified in tumor-bearing mice as $CD11b^{+}Gr1^{+}$ cells; they are a heterogeneous cellular population containing macrophages, granulocytes, immature DCs and immature myeloid cells.[22,23] They suppress T-cell responses *in vitro* through direct cell-cell contact or by producing arginase I and iNOS.[24] Antigen-specific CD8 T cell tolerance can be induced by nitration of the TCR-CD8 complex mediated by ROS and peroxynitrite produced by MDSCs.[18] They are divided into two populations: monocytic MDSC and granulocytic MDSC[25] which use different effector molecules and signals to suppress antigen-specific T cell responses. In monocytic MDSCs, IFN-γ signaling through STAT1 results in the production of NO.[26] In contrast, granulocytic MDSCs use ROS for their suppressive function.[18] Consistently, in our study, stronger ROS fluorescence intensity was seen in granulocytic MDSCs than monocytic MDSCs (Fig. 3*b*). In ACT, the recruitment of monocytic MDSCs into the tumor

as a result of CTL tumor infiltration outnumbered granulocytic MDSCs (Fig. 2). Therefore, the immunosuppressive activity of CTL-induced monocytic MDSC accumulation was mediated mainly by iNOS, partly by ROS or arginase I (Fig. 4). Both the absolute number of monocytic MDSCs (Fig. 2*b*) and the per cell expression of iNOS mRNA (Fig. 3*a*) were markedly increased in the tumor by ACT, treatment-induced immunosuppressive microenvironment in the tumor turned tougher than that of steady state condition.

We have reported that the robust induction of IFN-γ mRNA and IFN-γ-producing CTLs can be detected in tumors after ACT.[12] Because IFN-γ is a key effector molecule for CTL anti-tumor activity,[27] we investigated its contribution in our B16-pmel-1 CTL model. CTL-inhibited tumor growth was completely prevented by anti-IFN-γ mAb treatment (Fig. 5). This treatment also prevented the accumulation of monocytic MDSC in the tumor in CTL-treated mice. These results suggested that both suppression of tumor growth and the accumulation of monocytic MDSC at the tumor site were functionally dependent on IFN-γ. This is consistent with the report by Gallina *et al.* that MDSC activity was enhanced by IFN-γ released from activated T cells.[28] Monocytes conditioned by tumors express IL-4Rα and secrete IL-13. These two cytokines amplify the expression of iNOS and arginase, which mediate immunosuppression. Consistently, our study demonstrated that IFN-γ produced by adoptively-transferred antigen-specific CTLs augmented immunosuppressive activities of MDSCs in the quantitative as well as the qualitative sense (Figs. 1–3).

To separate anti-tumor activity of ACT from the pro-tumor immunosuppressive activity of MDSC, we studied events downstream of IFN-γ production, notably which chemokine system was involved in this process. It has been reported that the CCL2/CCR2 pathway mediates recruitment of MDSCs into cancers.[29,30] We had previously reported that the CCL2/CCR2 pathway mediates recruitment of myeloid suppressor cells to cancers by controlling both the mobilization of monocytes from the bone marrow to the blood and their migration to the tumor.[20] Although CX3CR1 and CCR5 are also known to be involved in the regulation of monocyte migration,[31,32] tumor-infiltrating macrophages were not reduced in CX3CR1$^{-/-}$ mice and no significant difference was observed in the efficiency of infiltration into tumors by adoptively transferred CCR5$^{+/-}$ and CCR5$^{-/-}$ bone marrow monocytes.[20] In the present study, we demonstrated that monocytic MDSCs recruited into the tumor after ACT strongly express CCR2 (Fig. 5*f*) and CCR2 ligands were induced in the tumor by ACT (Fig. 5*g*). We also demonstrated that ACT induced more profound anti-tumor effects in B16 tumor-bearing CCR2$^{-/-}$ mice in the absence of monocytic MDSC expansion than in wild-type mice (Fig. 6). These results were consistent with previous report of Lesokhin *et al.* that CCR2^{+} monocytic MDSCs accumulated in the GM-CSF secreting tumor and regulated the efficacy of CD8^{+} T cell therapy.[33] Fridlender *et al.* also reported that CCL2 blockade augments cancer immunotherapy.[34] Consistent with our results, anti-CCL2/CCL12 mAb treatment generated more intratumoral CD8^{+} T cells; however, no changes were observed in CD11b^{+}Ly6G^{+} granulocytic MDSCs or in the CD11b^{+}Ly6C^{+} monocytic MDSCs in their model. It remains to be determined whether and which factors might affect recruitment of MDSC subpopulations after ACT, but clearly CCL2, 7 and 12/CCR2 plays an important role in the accumulation of monocytic MDSC at the tumor site associated with ACT.

Despite the presence of granulocytic MDSC in the tumor after ACT possibly compensating for the reduction of monocytic MDSC in CCR2$^{-/-}$ mice, the anti-tumor activity of the infused CTL was not hampered and tumor growth remained profoundly suppressed. This supports the notion that monocytic MDSC, not granulocytic MDSC, were responsible for the ACT-associated immunosuppression. In line with our results, it has been reported that depletion of immune cells in mice before ACT improved the anti-tumor activity of the treatment.[35,36] Nonmyeloablative lymphodepleting preconditioning by systemic chemotherapy also markedly improved the efficacy of adoptive transfer of tumor infiltrating lymphocytes in melanoma patients.[37,38] The ACT-induced recruitment of MDSCs is presumably prevented under these conditions, because myelopoiesis *per se* was inhibited by preconditioning chemotherapy before ACT.

Recently, Landsberg *et al.* reported that melanoma cells acquired ACT resistance through a mechanism involving IFN-γ-dependent PD-L1 upregulation and TNF-α-dependent reversible loss of melanocytic antigens.[39] These two functionally related CTL-induced adaptive mechanisms together contributed to tumor resistance to ACT. Here, we demonstrated that IFN-γ-dependent secondary accumulation of monocytic MDSCs at the tumor site was also involved in this inhibitory process and further amplified the immunosuppressive network.

In conclusion, dual effects of CTL therapy, suppression of tumor growth and but also stimulation of monocytic MDSCs in the tumor, were both mediated by the IFN-γ produced by the infused tumor-specific CTLs. Considering that ACT triggered counter-regulatory immunosuppressive mechanism *via* recruitment of MDSCs, strategies for regulating this step are desired for optimizing ACT.

Acknowledgements

We thank Dr. Nicholas Restifo (National Cancer Institute) for providing the B16F10 tumor cell line, and Takuma Kono for technical assistance.

References

1. Rosenberg SA, Restifo NP, Yang JC, et al. Adoptive cell transfer: a clinical path to effective cancer immunotherapy. *Nat Rev* 2008;8:299–308.
2. Brenner MK, Heslop HE. Adoptive T cell therapy of cancer. *Curr Opin Immunol* 2010;22:251–7.
3. Morgan RA, Dudley ME, Wunderlich JR, et al. Cancer regression in patients after transfer of genetically engineered lymphocytes. *Science* 2006;314:126–9.
4. Robbins PF, Morgan RA, Feldman SA, et al. Tumor regression in patients with metastatic synovial cell sarcoma and melanoma using genetically engineered lymphocytes reactive with NY-ESO-1. *J Clin Oncol* 2011;29:917–24.
5. Kohn DB, Dotti G, Brentjens R, et al. CARs on track in the clinic. *Mol Ther* 2011;19:432–8.

6. Jena B, Dotti G, Cooper LJ. Redirecting T-cell specificity by introducing a tumor-specific chimeric antigen receptor. *Blood* 2010;116:1035–44.
7. Kalos M, Levine BL, Porter DL, et al. T cells with chimeric antigen receptors have potent antitumor effects and can establish memory in patients with advanced leukemia. *Sci Transl Med* 2011;3: 95ra73.
8. Sadelain M. T-cell engineering for cancer immunotherapy. *Cancer J* 2009;15:451–5.
9. Zou W. Immunosuppressive networks in the tumour environment and their therapeutic relevance. *Nat Rev* 2005;5:263–74.
10. Rabinovich GA, Gabrilovich D, Sotomayor EM. Immunosuppressive strategies that are mediated by tumor cells. *Annu Rev Immunol* 2007;25: 267–96.
11. Overwijk WW, Theoret MR, Finkelstein SE, et al. Tumor regression and autoimmunity after reversal of a functionally tolerant state of self-reactive CD8+ T cells. *J Exp Med* 2003;198:569–80.
12. Noji S, Hosoi A, Takeda K, et al. Targeting spatiotemporal expression of CD137 on tumor-infiltrating cytotoxic T lymphocytes as a novel strategy for agonistic antibody therapy. *J Immunother* 2012;35:460–72.
13. Boring L, Gosling J, Chensue SW, et al. Impaired monocyte migration and reduced type 1 (Th1) cytokine responses in C-C chemokine receptor 2 knockout mice. *J Clin Invest* 1997;100:2552–61.
14. Lutz MB, Kukutsch N, Ogilvie AL, et al. An advanced culture method for generating large quantities of highly pure dendritic cells from mouse bone marrow. *J Immunol Methods* 1999; 223:77–92.
15. Betts MR, Brenchley JM, Price DA, et al. Sensitive and viable identification of antigen-specific CD8+ T cells by a flow cytometric assay for degranulation. *J Immunol Methods* 2003;281: 65–78.
16. Eruslanov E, Kusmartsev S. Identification of ROS using oxidized DCFDA and flow-cytometry. *Methods Mol Biol* 2010;594:57–72.
17. Ueha S, Murai M, Yoneyama H, et al. Intervention of MAdCAM-1 or fractalkine alleviates graft-versus-host reaction associated intestinal injury while preserving graft-versus-tumor effects. *J Leukoc Biol* 2007;81:176–85.
18. Nagaraj S, Gupta K, Pisarev V, et al. Altered recognition of antigen is a mechanism of CD8+ T cell tolerance in cancer. *Nat Med* 2007;13:828–35.
19. Youn JI, Nagaraj S, Collazo M, et al. Subsets of myeloid-derived suppressor cells in tumor-bearing mice. *J Immunol* 2008;181:5791–802.
20. Sawanobori Y, Ueha S, Kurachi M, et al. Chemokine-mediated rapid turnover of myeloid-derived suppressor cells in tumor-bearing mice. *Blood* 2008;111:5457–66.
21. Hanahan D, Weinberg RA. Hallmarks of cancer: the next generation. *Cell* 2011;144:646–74.
22. Peranzoni E, Zilio S, Marigo I, et al. Myeloid-derived suppressor cell heterogeneity and subset definition. *Curr Opin Immunol* 2010;22:238–44.
23. Gabrilovich DI, Ostrand-Rosenberg S, Bronte V. Coordinated regulation of myeloid cells by tumours. *Nat Rev Immunol* 2012;12:253–68.
24. Talmadge JE. Pathways mediating the expansion and immunosuppressive activity of myeloid-derived suppressor cells and their relevance to cancer therapy. *Clin Cancer Res* 2007;13:5243–8.
25. Gabrilovich DI, Nagaraj S. Myeloid-derived suppressor cells as regulators of the immune system. *Nat Rev Immunol* 2009;9:162–74.
26. Movahedi K, Guilliams M, Van den Bossche J, et al. Identification of discrete tumor-induced myeloid-derived suppressor cell subpopulations with distinct T cell-suppressive activity. *Blood* 2008;111:4233–44.
27. Schreiber RD, Old LJ, Smyth MJ. Cancer immunoediting: integrating immunity's roles in cancer suppression and promotion. *Science* 2011;331: 1565–70.
28. Gallina G, Dolcetti L, Serafini P, et al. Tumors induce a subset of inflammatory monocytes with immunosuppressive activity on CD8+ T cells. *J Clin Invest* 2006;116:2777–90.
29. Huang B, Lei Z, Zhao J, et al. CCL2/CCR2 pathway mediates recruitment of myeloid suppressor cells to cancers. *Cancer Lett* 2007;252:86–92.
30. Qian BZ, Li J, Zhang H, et al. CCL2 recruits inflammatory monocytes to facilitate breast-tumour metastasis. *Nature* 2011;475:222–5.
31. Geissmann F, Jung S, Littman DR. Blood monocytes consist of two principal subsets with distinct migratory properties. *Immunity* 2003;19:71–82.
32. Tacke F, Alvarez D, Kaplan TJ, et al. Monocyte subsets differentially employ CCR2, CCR5, and CX3CR1 to accumulate within atherosclerotic plaques. *J Clin Invest* 2007;117:185–94.
33. Lesokhin AM, Hohl TM, Kitano S, et al. Monocytic CCR2(+) myeloid-derived suppressor cells promote immune escape by limiting activated CD8 T-cell infiltration into the tumor microenvironment. *Cancer Res* 2012;72:876–86.
34. Fridlender ZG, Buchlis G, Kapoor V, et al. CCL2 blockade augments cancer immunotherapy. *Cancer Res* 2010;70:109–18.
35. Cheever MA, Greenberg PD, Fefer A. Specificity of adoptive chemoimmunotherapy of established syngeneic tumors. *J Immunol* 1980;125: 711–14.
36. North RJ. Cyclophosphamide-facilitated adoptive immunotherapy of an established tumor depends on elimination of tumor-induced suppressor T cells. *J Exp Med* 1982;155:1063–74.
37. Dudley ME, Wunderlich JR, Robbins PF, et al. Cancer regression and autoimmunity in patients after clonal repopulation with antitumor lymphocytes. *Science* 2002;298:850–4.
38. Dudley ME, Wunderlich JR, Yang JC, et al. Adoptive cell transfer therapy following non-myeloablative but lymphodepleting chemotherapy for the treatment of patients with refractory metastatic melanoma. *J Clin Oncol* 2005;23: 2346–57.
39. Landsberg J, Kohlmeyer J, Renn M, et al. Melanomas resist T-cell therapy through inflammation-induced reversible dedifferentiation. *Nature* 2012;490:412–16.

Granulocyte macrophage colony-stimulating factor as a predictor of the response of metastatic renal cell carcinoma to tyrosine kinase inhibitor therapy

DAISUKE YAMADA[1], HIROKAZU MATSUSHITA[2], TAKESHI AZUMA[3], TOHRU NAKAGAWA[3], MASAYOSHI NAGATA[4], YUKIO YAMADA[3], MOTOFUMI SUZUKI[4,5], TETSUYA FUJIMURA[3], HIROSHI FUKUHARA[3], HARUKI KUME[3], YUKIO HOMMA[3] and KAZUHIRO KAKIMI[2]

[1]Department of Urology, Chibanishi General Hospital, Matsudo, Chiba 270-2251; Departments of [2]Immunotherapeutics and [3]Urology, University of Tokyo Hospital, Tokyo 113-8655; [4]Department of Urology, National Center for Global Health and Medicine, Tokyo 162-8655; [5]Department of Urology, Tokyo Teisin Hospital, Tokyo 102-8798, Japan

Received June 12, 2014; Accepted July 7, 2014

DOI: 10.3892/mco.2014.360

Abstract. This prospective study was conducted to identify predictive markers for the response of metastatic renal cell carcinoma (RCC) to tyrosine kinase inhibitors (TKIs). Patients with histologically proven RCC with at least one measurable metastatic lesion were enrolled in this study. Blood samples were collected prior to treatment and the plasma levels of 27 cytokines were measured. Tumor response was assessed 8-12 weeks after the initiation of TKI treatment. A total of 13 patients (11 men and 2 women) with a median age of 63 years received sunitinib (8 cases), sorafenib (1 case), or axitinib (4 cases). Partial response (PR) was achieved in 5 patients (38%), stable disease (SD) in 4 (30%) and progressive disease (PD) was noted in 4 (30%). The plasma granulocyte macrophage colony-stimulating factor (GM-CSF) level in PR cases was significantly higher compared to that in SD or PD cases (P=0.012). Therefore, GM-CSF may be a predictive biomarker of the response of RCC to TKI treatment, suggesting that TKIs may exert clinical effects not only through suppression of the vascular endothelial growth factor, but also through immune system modulation.

Introduction

Renal cell carcinoma (RCC) is one of the major causes of cancer-related mortality. There were an estimated ~64,700 new cases of RCC and 13,570 deaths in 2012 in the United States (1). Over the last few years, a number of tyrosine kinase inhibitors (TKIs) have been proven to be effective and are currently widely used for the treatment of metastatic RCC. However, the effect of these TKIs appears to be rather limited, with only 31% of naive cases exhibiting an objective response [complete response (CR) or partial response (PR)] to sunitinib treatment in the first-line setting (2) and only 10% of cases with previous cytokine therapy exhibiting a PR to treatment with sorafenib (3). However, thus far, only a limited number of factors that predict the response of RCC to TKIs have been reported. A significant decrease in serum vascular endothelial growth factor (VEGF) receptor-2 levels and/or an increase in serum VEGF levels were observed in patients exhibiting an objective tumor response (4,5). Hypothyroidism and hypertension associated with TKI treatment were also reported to be correlated with a favorable response (6,7).

Although previous studies suggested that TKIs may affect the immune system (8,9), only a limited number of studies have investigated immunological biomarkers for therapeutic prediction. Adotevi *et al* (10) reported that a decrease in regulatory T cells was correlated with a favorable overall survival in cases with metastatic RCC who received sunitinib-based antiangiogenic therapy. Thus, we conducted a prospective study to invesigate predictive immunological biomarkers.

Patients and methods

Patients. Patients with histologically proven RCC with at least one measurable metastatic lesion, who were diagnosed between March, 2012 and June, 2013, were enrolled in this study. Sunitinib, sorafenib or axitinib were administered orally as previously described (2,3,11). Tumor response was assessed 8-12 weeks after the initiation of TKI treatment according to the response evaluation criteria in solid tumors and was classified as CR, PR, stable disease (SD) or progressive disease (PD) (12).

We collected blood samples from the 13 patients prior to treatment. The plasma was deep frozen at -80°C and stored before measuring the immune function.

Cytokines. A total of 27 cytokines including interleukin (IL)-1β, IL-1ra, IL-2, IL-4, IL-5, IL-6, IL-7, IL-8, IL-9,

Correspondence to: Dr Haruki Kume, Department of Urology, University of Tokyo Hospital, 7-3-1 Hongo, Bunkyo-ku, Tokyo 113-8655, Japan
E-mail: kume@kuc.biglobe.ne.jp

Key words: metastatic, renal cell carcinoma, tyrosine kinase inhibitors, granulocyte macrophage colony-stimulating factor

Table I. Correlation between the clinical effect of tyrosine kinase inhibitors (TKIs) and clinicopathological characteristics among patients with metastatic renal cancer.

Clinical characteristics	Total (n=13)	Clinical effect[a] PR (n=5)	SD (n=4)	PD (n=4)	P-value
Gender					
Male	11	4	4	3	0.603
Female	2	1	0	1	
Age (years)					
≥65	7	2	2	3	0.593
<65	6	3	2	1	
Performance status					
0	8	3	2	3	0.780
1	5	2	2	1	
Laterality					
Right	8	2	3	3	0.479
Left	5	3	1	1	
Nephrectomy					
Radical	11	4	4	3	0.603
Partial	2	1	0	1	
Histology					
Clear cell RCC	11	5	2	4	0.085
Papillary RCC	2	0	2	0	
Nuclear grade					
G1/G2	12	4	4	4	0.449
G3	1	1	0	0	
Stage					
pT1	6	3	1	2	0.593
pT2/pT3/pT4	7	2	3	2	
Lymphovascular invasion					
0	2	1	1	0	0.603
1	11	4	3	4	
Lung metastasis					
No	3	1	2	0	0.267
Yes	10	4	2	4	
Bone metastasis					
No	8	2	4	2	0.180
Yes	5	3	0	2	
TKIs					
Sunitinib	8	4	3	1	0.219
Others	5	1	1	3	
Dose intensity (%)					
100	7	2	2	3	0.593
<100	6	3	2	1	
Previous treatment					
No	2	1	1	0	0.603
Yes	11	4	3	4	
Previous TKI treatment					
No	8	4	3	1	0.219
Yes	5	1	1	3	
Previous cytokine treatment					
No	5	3	1	1	0.479
Yes	8	2	3	3	

Table I. Continued.

Clinical characteristics	Total (n=13)	Clinical effect[a] PR (n=5)	SD (n=4)	PD (n=4)	P-value
Previous mTOR inhibitor treatment					
No	10	4	3	3	0.980
Yes	3	1	1	1	

[a]Best response during the 3-month treatment. The P-values were calculated using the Kruskal-Wallis test. PR, partial response; SD, stable disease; PD, progressive disease; RCC, renal cell carcinoma; mTOR, mammalian target of rapamycin.

IL-10, IL-12, IL-13, IL-15, IL-17, eotaxin, basic fibroblast growth factor, granulocyte colony-stimulating factor, granulocyte macrophage colony-stimulating factor (GM-CSF), interferon-γ (IFN-γ), IFN-γ-induced protein 10, monocyte chemoattractant protein-1, macrophage inflammatory protein (MIP)-1α, platelet-derived growth factor (PDGF)-BB, MIP-1β, regulated on activation, normal T-cell expressed and secreted, tumor necrosis factor-α and VEGF were measured twice by BioPlex Pro Human Cytokine 27 Plex assay (M50-0KCAF0Y; Bio-Rad, Hercules, CA, USA). The assay was performed according to the manufacturer's instructions. Briefly, plasma was centrifuged at 15,000 x g for 10 min at 4˚C. The samples were then incubated with microbeads labeled with specific antibodies to one of the aforementioned cytokines for 60 min. Following a washing step, the beads were incubated with the detection antibody cocktail, with each antibody specific to a single cytokine, for 30 min. After another washing step, the beads were incubated with streptavidin-phycoerythrin for 10 min, washed again and the concentration of each cytokine was determined using the array reader. The samples were tested in duplicate on a 96-well plate alongside the standard curve used to generate the results. Unknown concentrations were calculated from a standard curve generated from Bio-Rad supplied standards.

Statistical analysis. The correlation between clinical and cytokine data was analyzed by analysis of variance (ANOVA) and Tukey-Kramer's test using JMP software, version 10.0.0 (SAS, Institute, Cary, NC, USA).

This study was approved by the Institutional Ethics Committee of the Faculty of Medicine and Graduate School of Medicine of the University of Tokyo (no. H22-23-400).

Results

Patient characteristics. A total of 13 patients (8 treated with sunitinib, 1 with sorafenib and 4 with axitinib), including 11 men and 2 women, with a median age of 63 years (range, 50-77 years), were recruited in this study (Table I). The performance status was 0 in 8 and 1 in 5 cases. Eight tumors were located in the right and 5 in the left kidney. Radical nephrectomy was performed in 11 and partial nephrectomy in 2 patients. Histologically, the tumors were diagnosed as 11 clear cell RCCs and 2 papillary RCCs. All the patients had developed metastasis, with the most common metastatic site being the lung (10 cases), followed by bone (5 cases).

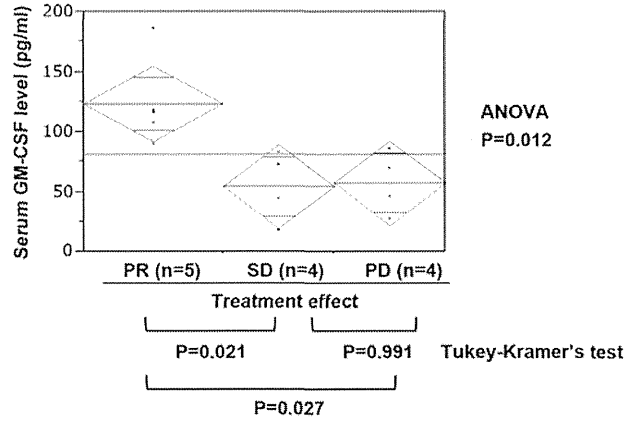

Figure 1. Comparison of serum granulocyte macrophage colony-stimulating factor (GM-CSF) levels among patients who achieved partial response (PR), stable disease (SD) or exhibited progressive disease (PD) after treatment with tyrosine kinase inhibitors. ANOVA, analysis of variance.

Treatment. Two cases received TKI treatment as first-line therapy. Previous systemic treatment included TKIs in 5, mammalian target of rapamycin (mTOR) inhibitors in 3 and cytokines in 8 patients. PR was achieved in 5 cases (38%), SD in 4 (30%) and PD developed in 4 cases (30%). The dose was reduced in 6 patients (46%) due to adverse events.

GM-CSF plasma levels by treatment response. No clinical parameters exhibited a significant correlation with treatment effect (Table I). Among the 27 investigated cytokines, the plasma GM-CSF level in PR cases was significantly higher compared to that in cases with SD or PD (Fig. 1, ANOVA, P=0.012; Tukey-Kramer's test: PR vs. SD, P=0.021; PR vs. PD, P=0.027; and SD vs. PD, P=0.991). The IL-6 level was higher in PD cases, but the difference was not statistically significant (Table II, P=0.141).

Discussion

We demonstrated that plasma GM-CSF may be a predictive marker of the response to TKI treatment. Thus far, only a few studies demonstrated the clinical utility of GM-CSF. The

Table II. Correlation between the clinical effect of tyrosine kinase inhibitors and cytokine levels in patients with metastatic renal cancer.

	Clinical effect			
Cytokines	PR	SD	PD	P-value
GM-CSF	123±36	54±29	57±25	0.012
IL-1β	3.8±4.6	1.9±1.2	1.6±0.2	0.494
IL-1ra	103±98	57±43	60±22	0.536
IL-2	5.2±2	4.8±3.1	5±3	0.971
IL-4	5.6±2.3	4.8±1.8	5.1±2.2	0.864
IL-5	1.1±1.4	0.7±0.8	0.6±0.8	0.791
IL-6	6±2.3	5±2.6	12±8.9	0.141
IL-7	5.3±1.9	4.8±4.9	3.1±2.2	0.605
IL-8	25±13	29±33	19±12	0.779
IL-9	44±12	26±8.8	29±15	0.125
IL-10	4.2±2.9	3.4±1.1	6.4±5.7	0.525
IL-12	19±17	17±15	32±37	0.658
IL-13	5.2±3.9	5.1±3.1	5.1±2.4	0.990
IL-15	5±1.6	3.6±2.3	4.2±0.6	0.479
IL-17	56±15	41±16	59±41	0.613
Eotaxin	183±152	128±126	112±61	0.667
FGF-basic	51±14	42±12	55±22	0.554
G-CSF	66±19	52±18	59±13	0.527
IFN-γ	610±893	207±94	178±21	0.462
IP-10	2,381±1,857	1,386±749	1,906±1,432	0.616
MCP-1	82±68	41±16	47±22	0.388
MIP-1α	2.9±1.1	7.7±12	2.9±1.7	0.561
PDGF-BB	309±306	862±146	213±128	0.508
MIP-1β	178±43	174±141	128±79	0.703
RANTES	3,364±138	2,630±763	2,679±771	0.523
TNF-α	88±92	62±47	43±6.9	0.580
VEGF	108±62	122±79	165±143	0.683

The results are expressed as mean ± standard deviation (pg/ml) and the P-values were calculated using analysis of variance. PR, partial response; SD, stable disease; PD, progressive disease; GM-CSF, granulocyte macrophage colony-stimulating factor; IL, interleukin; FGF, fibroblast growth factor; G-CSF, granulocyte colony-stimulating factor; IFN-γ, interferon-γ; IP-10, IFN-γ-induced protein 10; MCP-1, monocyte chemoattractant protein-1; MIP, macrophage inflammatory protein; RANTES, regulated on activation, normal T-cell expressed and secreted; PDGF, platelet-derived growth factor; TNF-α, tumor necrosis factor-α; VEGF, vascular endothelial growth factor.

plasma GM-CSF level was found to be higher in cervical cancer patients compared to healthy controls (13), while in another study GM-CSF was undetectable in non-cancer patients (14).

GM-CSF promotes the differentiation and expansion of myeloid-derived suppressor cells (MDSCs) (15,16). Antigen-specific $CD8^+$ T-cell tolerance, induced by MDSCs, is known to be one of the main mechanisms of tumor escape (17). Knockdown of GM-CSF in tumor cells may reverse the cytotoxicity to CD8 T lymphocytes: Dolcetti *et al* (15) found that lack of GM-CSF release from 4T1 mammary carcinoma cells reduced the accumulation of $Gr\text{-}1^{int/low}$ MDSC subsets and successfully inhibited tumor-induced tolerance in mice. Similarly, Serafini *et al* (16) demonstrated that inhibition of MDSC function abrogates the proliferation of regulatory T cells and tumor-induced tolerance in antigen-specific T cells, using the A20 B-cell lymphoma model *in vitro* and *in vivo*. However, TKIs may reduce the number of MDSCs in the tumor and normalize T-lymphocyte function: Xin *et al* (18) demonstrated that sunitinib directly induced RCC tumor cell apoptosis through Stat3 inhibition, which was accompanied by a reduction in MDSCs and tumor-infiltrating regulatory T cells.

These reports suggest that high levels of plasma GM-CSF may promote the function of MDSCs and escape of tumor cells from the host immune system. In patients with high GM-CSF levels, TKIs may decrease the function of MDSCs that is upregulated by GM-CSF and reverse the cytotoxicity of regulatory T lymphocytes directly or indirectly, which may lower tumor-induced tolerance and result in favorable treatment effects.

In our study, VEGF was not found to be significantly associated with treatment effect, contrary to previous reports (4,5). GM-CSF was reported to induce VEGF release from the epithelium, resulting in the promotion of carcinogenesis: Wang *et al* (19) demonstrated that, in a colitis-associated cancer model, blocking GM-CSF activity *in vivo* significantly decreased epithelial release of VEGF and abrogated cancer formation. In the plasma, GM-CSF, which is upstream of VEGF, may be a more sensitive biomarker for metastatic RCC treatment compared to VEGF.

As regards other biomarkers, Tran *et al* (20) screened pretreatment cytokines and angiogenic factors in patients with metastatic RCC who received pazopanib treatment and found that high IL-6 was predictive for unfavorable progression-free survival. In our study, IL-6 was also higher in PD cases, but the difference was not statistically significant.

This study had certain limitations. First, this was a single-institution study; and second, our sample size was limited.

In conclusion, high pre-treatment plasma levels of GM-CSF, which is an inducer of immune tolerance, were significantly associated with a favorable response of metastatic RCC to TKI treatment. The result suggests the potential of GM-CSF as a predictive biomarker of the response to TKI treatment. However, further investigation is required to determine the effects of TKIs on abrogating cancer immune tolerance.

References

1. Siegel R, Naishadham D and Jemal A: Cancer statistics, 2012. CA Cancer J Clin 62: 10-29, 2012.
2. Motzer RJ, Hutson TE, Tomczak P, *et al*: Sunitinib versus interferon alfa in metastatic renal-cell carcinoma. N Engl J Med 356: 115-124, 2007.
3. Escudier B, Eisen T, Stadler WM, *et al*; TARGET Study Group: Sorafenib in advanced clear-cell renal-cell carcinoma. N Engl J Med 356: 125-134, 2007.
4. Shoji S, Nakano M, Sato H, Tang XY, Osamura YR, Terachi T, Uchida T and Takeya K: The current status of tailor-made medicine with molecular biomarkers for patients with clear cell renal cell carcinoma. Clin Exp Metastasis 31: 111-134, 2013.

5. Deprimo SE, Bello CL, Smeraglia J, Baum CM, Spinella D, Rini BI, Michaelson MD and Motzer RJ: Circulating protein biomarkers of pharmacodynamic activity of sunitinib in patients with metastatic renal cell carcinoma: modulation of VEGF and VEGF-related proteins. J Transl Med 5: 32, 2007.
6. Rini BI, Cohen DP, Lu DR, Chen I, Hariharan S, Gore ME, Figlin RA, Baum MS and Motzer RJ: Hypertension as a biomarker of efficacy in patients with metastatic renal cell carcinoma treated with sunitinib. J Natl Cancer Inst 103: 763-773, 2011.
7. Clemons J, Gao D, Naam M, Breaker K, Garfield D and Flaig TW: Thyroid dysfunction in patients treated with sunitinib or sorafenib. Clin Genitourin Cancer 10: 225-231, 2012.
8. Wongkajornsilp A, Wamanuttajinda V, Kasetsinsombat K, Duangsa-ard S, Sa-ngiamsuntorn K, Hongeng S and Maneechotesuwan K: Sunitinib indirectly enhanced anti-tumor cytotoxicity of cytokine-induced killer cells and $CD3^+CD56^+$ subset through the co-culturing dendritic cells. PLoS One 8: e78980, 2013.
9. Gu Y, Zhao W, Meng F, Qu B, Zhu X, Sun Y, Shu Y and Xu Q: Sunitinib impairs the proliferation and function of human peripheral T cell and prevents T-cell-mediated immune response in mice. Clin Immunol 135: 55-62, 2010.
10. Adotevi O, Pere H, Ravel P, *et al*: A decrease of regulatory T cells correlates with overall survival after sunitinib-based antiangiogenic therapy in metastatic renal cancer patients. J Immunother 33: 991-998, 2010.
11. Rini BI, Escudier B, Tomczak P, *et al*: Comparative effectiveness of axitinib versus sorafenib in advanced renal cell carcinoma (AXIS): a randomised phase 3 trial. Lancet 378: 1931-1939, 2011.
12. Eisenhauer EA, Therasse P, Bogaerts J, *et al*: New response evaluation criteria in solid tumours: revised RECIST guideline (version 1.1). Eur J Cancer 45: 228-247, 2009.
13. Lawicki S, Bedkowska GE, Gacuta-Szumarska E, Knapp P and Szmitkowski M: Pretreatment plasma levels and diagnostic utility of hematopoietic cytokines in cervical cancer or cervical intraepithelial neoplasia patients. Folia Histochem Cytobiol 50: 213-219, 2012.
14. Biancotto A, Wank A, Perl S, Cook W, Olnes MJ, Dagur PK, Fuchs JC, Langweiler M, Wang E and McCoy JP: Baseline levels and temporal stability of 27 multiplexed serum cytokine concentrations in healthy subjects. PLoS One 8: e76091, 2013.
15. Dolcetti L, Peranzoni E, Ugel S, *et al*: Hierarchy of immunosuppressive strength among myeloid-derived suppressor cell subsets is determined by GM-CSF. Eur J Immunol 40: 22-35, 2010.
16. Serafini P, Mgebroff S, Noonan K and Borrello I: Myeloid-derived suppressor cells promote cross-tolerance in B-cell lymphoma by expanding regulatory T cells. Cancer Res 68: 5439-5449, 2008.
17. Nagaraj S, Gupta K, Pisarev V, Kinarsky L, Sherman S, Kang L, Herber DL, Schneck J and Gabrilovich DI: Altered recognition of antigen is a mechanism of $CD8^+$ T cell tolerance in cancer. Nat Med 13: 828-835, 2007.
18. Xin H, Zhang C, Herrmann A, Du Y, Figlin R and Yu H: Sunitinib inhibition of Stat3 induces renal cell carcinoma tumor cell apoptosis and reduces immunosuppressive cells. Cancer Res 69: 2506-2513, 2009.
19. Wang Y, Han G, Wang K, *et al*: Tumor-derived GM-CSF promotes inflammatory colon carcinogenesis via stimulating epithelial release of VEGF. Cancer Res 74: 716-726, 2014.
20. Tran HT, Liu Y, Zurita AJ, *et al*: Prognostic or predictive plasma cytokines and angiogenic factors for patients treated with pazopanib for metastatic renal-cell cancer: a retrospective analysis of phase 2 and phase 3 trials. Lancet Oncol 13: 827-837, 2012.

Journal for
ImmunoTherapy of Cancer

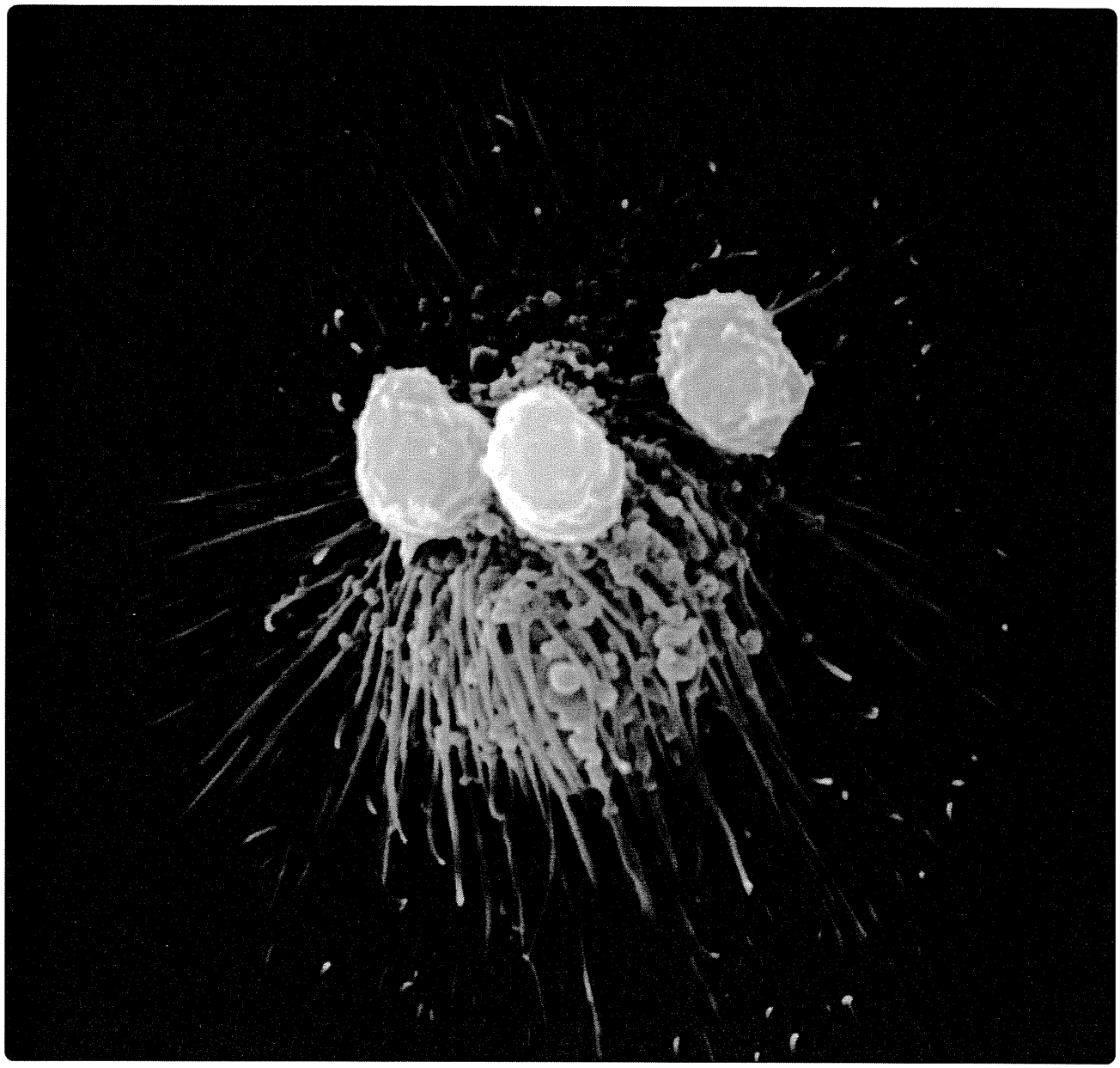

A pilot study of autologous tumor lysate-loaded dendritic cell vaccination combined with sunitinib for metastatic renal cell carcinoma

Matsushita *et al.*

BioMed Central

Matsushita *et al. Journal for ImmunoTherapy of Cancer* 2014, **2**:30
http://www.immunotherapyofcancer.org/content/2/1/30

Journal for ImmunoTherapy of Cancer

RESEARCH ARTICLE Open Access

A pilot study of autologous tumor lysate-loaded dendritic cell vaccination combined with sunitinib for metastatic renal cell carcinoma

Hirokazu Matsushita[1†], Yutaka Enomoto[2,3†], Haruki Kume[2], Tohru Nakagawa[2], Hiroshi Fukuhara[2], Motofumi Suzuki[2], Tetsuya Fujimura[2], Yukio Homma[2] and Kazuhiro Kakimi[1*]

Abstract

Background: Sunitinib, a tyrosine kinase inhibitor currently in use for the treatment of metastatic renal cell carcinoma (mRCC), has been reported to modulate immunosuppressive cells such as myeloid-derived suppressor cells (MDSCs) and regulatory T cells (Tregs) in addition to exerting anti-angiogenic effects. We conducted a clinical trial of dendritic cell (DC)-based immunotherapy together with sunitinib in mRCC patients in an effort to enhance immunotherapeutic efficacy by inhibiting immunosuppressive cells.

Methods: Patients aged ≥20 years with advanced or recurrent mRCC who underwent nephrectomy were eligible for this study. Autologous tumor samples were obtained by surgery under aseptic conditions and used for preparing autologous tumor lysate. About 4 weeks after surgery, leukapheresis was performed to isolate peripheral blood mononuclear cells (PBMCs). DCs were generated from adherent PBMCs in the presence of recombinant human granulocyte macrophage colony-stimulating factor (GM-CSF) (500 IU/ml) and recombinant human IL-4 (500 IU/ml). Autologous tumor lysate was loaded into mature DC by electroporation. Eight patients were enrolled in the study and received sunitinib at a dose of 50 mg p.o. daily for 28 days followed by 14 days of rest. Tumor lysate-loaded DCs were administered subcutaneously every two weeks, with concomitant sunitinib.

Results: No severe adverse events related to vaccination were observed. Sunitinib decreased the frequencies of MDSCs in peripheral blood of 5 patients and of Tregs in 3. Tumor lysate-reactive CD4 or CD8 T cell responses were observed in 5 patients, 4 of whom showed decreased frequencies of Tregs and/or MDSCs. The remaining 3 patients who failed to develop tumor-reactive T cell responses had high levels of IL-8 in their sera and did not show consistent reductions in MDSCs and Tregs.

Conclusions: DC-based immunotherapy combined with sunitinib is safe and feasible for patients with mRCC.

Trial registration: UMIN000002136

Keywords: RCC, Sunitinib, Dendritic cell, Lysate

Background

Renal cell carcinoma (RCC) accounts for 2–3% of all adult cancers. Approximately 20–30% of patients present with metastatic disease. Although surgery is the primary curative therapy for localized RCC, the prognosis for patients with advanced metastatic disease is poor, with a 5-year survival rate of <10% [1,2]. Since the first receptor tyrosine kinase inhibitor (TKI) sorafenib was approved for the treatment of cytokine-refractory metastatic RCC (mRCC), many agents have become available for the treatment of this disease. However, many tumors acquire resistance to these agents by mutating the target genes or activating other pathways that bypass the site of inhibition. This occurs rapidly, often within several months [3]. Therefore, development of other modalities such as immunotherapy is still needed for the treatment of mRCC.

* Correspondence: kakimi@m.u-tokyo.ac.jp
†Equal contributors
[1]Department of Immunotherapeutics, The University of Tokyo Hospital, 7-3-1 Hongo, Bunkyo-ku, Tokyo 113-8655, Japan
Full list of author information is available at the end of the article

RCC appears to be one of the most immune-sensitive cancers. This has encouraged the use of immunomodulating treatments such as cytokine-based therapy using IL-2 and/or interferon-α (IFN-α) [4,5]. Nonetheless, nephrectomy is still recommended for patients with mRCC [6], because cytoreductive therapy was shown to provide overall survival benefit in patients treated with IFN-α [7]. Although it is still controversial whether cytoreductive therapy also contributes to the efficacy of TKIs [8], nephrectomy reduces the tumor burden, alleviates symptoms and allows more information on histology to be acquired. In addition, we can utilize the resected tumor as a source of autologous materials, such as tumor lysates, for the production of autologous tumor vaccines. It has been reported that adjuvant treatment with autologous tumor lysate vaccine resulted in a significantly improved overall survival in pT3 stage RCC patients [9]. Antigen-specific vaccination with dendritic cells (DCs) has also been conducted, but with only limited success so far [10-15], possibly due to functionally-defective T cell responses in the tumor microenvironment.

It is well accepted that the tumor microenvironment imposes different degrees of immunosuppression allowing the tumor to evade immune responses [16]. These include the delivery of negative costimulatory signals to T cells (via PD-L1, B7-H4) and production of immunosuppressive factors (eg. IL-10, TGF-β, IDO and others). Recently, promising immunotherapeutic strategies have emerged from our understanding of immunoinhibitory pathways termed "immune checkpoints", which are crucial for maintaining self-tolerance and modulating the duration and magnitude of physiological immune responses. Tumors utilize such immune checkpoints as a resistance mechanism to escape anti-tumor immune responses [17]. Hence, immune checkpoint blockade is a promising approach to activating antitumor immunity. The antibodies that block CTLA-4- and PD-1-dependent interactions have been successfully applied for the treatment of mRCC [18-21].

In addition, different regulatory cell populations, such as MDSCs or Tregs, are involved in this process. The accumulation of MDSCs as well as the suppression of T-cell function in mRCC patients has been reported [22,23]. TKIs such as sunitinib and sorafenib were approved some time ago and are now the mainstay for the treatment of mRCC [24-26]. In addition to its anti-angiogenic effects, sunitinib has been demonstrated to modulate immunosuppressive MDSCs in human [27] and mouse [28]. It has also been reported that sunitinib reverses type-1 immune suppression and decreases Tregs in renal cell carcinoma patients [29]. Furthermore, sunitinib, unlike sorafenib, does not inhibit specific T cell responses [30]. Therefore, sunitinib appears to be a promising molecular target drug for combination therapy together with cancer vaccines for mRCC.

Here, we report the results of a clinical trial in which we evaluated the safety and feasibility of DC-based vaccination combined with sunitinib for mRCC patients and tested whether sunitinib enhances immune responses by reducing immunosuppressive cells.

Results

Patients

Eight patients (5 men and 3 women) with a median age of 68 yr (range, 55–75) were enrolled in this study (Table 1). Two patients were categorized into the MSKCC poor risk group and the other six as having an intermediate risk. One patient (#1808) had unclassified RCC, while the other seven had clear cell RCC. Two patients, #1802 and #1803, received sunitinib or IFN-α and radiation for bone metastasis, respectively, before surgery.

DC Vaccine combined with sunitinib

DCs were successfully generated from all 8 patients (Table 2). Final concentrations of tumor lysate per 10^7 DCs ranged from 0.44 to 1.33 mg (mean value, 0.90 mg). Flow cytometric analysis of the harvested tumor lysate-loaded DCs revealed a phenotype characteristic of mature DCs with high expression of CD40, CD80, CD83, CD86, HLA-ABC, HLA-DR, and CCR7 (Figure 1 and Table 3). While there were some differences in the fluorescent intensities of these molecules among patients' DCs (Additional file 1), the phenotype of these DCs were quite comparable. None of the DC preparations was microbially contaminated. Each patient was given 1×10^7 DCs at each time point, with the exception of one patient (#1823) who received 0.5×10^7 DCs (Table 2). Patients received 6 vaccinations and sunitinib at a dose of 50 mg p.o. daily for 28 days followed by 14 days of rest, according to the schedule (Additional file 2). Vaccination was well-tolerated and no severe vaccination-related toxicity or autoimmune manifestations were observed in any patient.

Frequencies of MDSCs and Tregs in peripheral blood

MDSCs in peripheral blood were evaluated by two criteria (percent of $CD14^-CD15^+$ or $CD33^+HLA\text{-}DR^-$ cells within the $Dye780^-CD45^+$ population) (Additional file 3). In individual patients, decreased percentages of MDSCs were observed in 5 of the 8 patients (#1802, #1803, #1806, #1814, and #1823) by both criteria (Figure 2A and Table 4) compared to pretreatment baseline. No marked changes were observed in patients #1808, #1812 and #1817. Sunitinib significantly reduced the average percentage of $CD14^-CD15^+$ MDSCs in 8 patients from 0.62 ± 1.20% (mean ± SD) at the baseline to 0.083 ± 0.17% at the 6th DC injection ($p = 0.0039$, Wilcoxon signed-rank test); the average percentage of $CD33^+HLA\text{-}DR^-$ MDSCs in 8 patients did not change (2.57 ± 2.86% at the baseline and 3.17 ± 6.73%